

This document is confidential and is proprietary to the American Chemical Society and its authors. Do not copy or disclose without written permission. If you have received this item in error, notify the sender and delete all copies.

Customized Synthesis: Solvent- and Acid-Assisted Topology Evolution in Zirconium-Tetracarboxylate Frameworks

Journal:	<i>Inorganic Chemistry</i>
Manuscript ID	ic-2022-00660n.R2
Manuscript Type:	Article
Date Submitted by the Author:	25-Apr-2022
Complete List of Authors:	Xia, Hai-Lun; Shenzhen Polytechnic Zhou, Kang; Shenzhen Polytechnic Yu, Liang; Shenzhen Polytechnic, Hoffmann Institute of Advanced Materials Wang, Hao; Shenzhen Polytechnic, Hoffmann Institute of Advanced Materials Liu, Xiao-Yuan; Shenzhen Polytechnic, Hoffmann Institute of Advanced Materials Proserpio, Davide; Universita degli Studi di Milano, Dipartimento di Chimica Li, Jing; Rutgers The State University of New Jersey, Chemistry and Chemical Biology; Rutgers The State University of New Jersey, Chemistry and Chemical Biology

SCHOLARONE™
Manuscripts

Customized Synthesis: Solvent- and Acid-Assisted Topology Evolution in Zirconium-Tetracarboxylate Frameworks

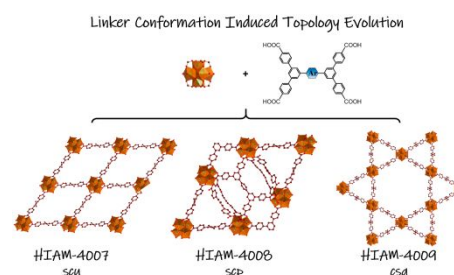
Hai-Lun Xia,[†] Kang Zhou,[†] Liang Yu,[†] Hao Wang,[†] Xiao-Yuan Liu,^{*,†} Davide M. Proserpio,[‡] Jing Li^{*,§,†}

[†] Hoffmann Institute of Advanced Materials, Shenzhen Polytechnic, 7098 Liuxian Blvd, Nanshan District, Shenzhen, 518055, P.R. China

[‡] Dipartimento di Chimica, Università degli Studi di Milano, Milano 20133, Italy

[§] Department of Chemistry and Chemical Biology, Rutgers University, 123 Bevier Road, Piscataway, New Jersey 08854, United States

ABSTRACT: Metal-organic frameworks (MOFs) demonstrate strong potential for various important applications due to their well tunable structures and compositions through metal- and organic linker-engineering. As an effective approach, topology evolution by controlling linker conformation has received considerable attention, where solvents and acids make crucial effects on structural formation. However, a systematic study of such effect remains under investigated. Herein, we carried out a methodical study on the topology evolution in Zr-MOFs directed by solvothermal conditions with various combinations of three common solvents and six different acids. As a result, three Zr-MOFs with different topologies, **scu** (HIAM-4007), **scp** (HIAM-4008) and **csq** (HIAM-4009), were obtained using the same Zr₆-cluster and tetratopic carboxylate linker, in which structure diversity shows significant influence on their corresponding photoluminescence quantum yields. Further experiments revealed that the acidity of acid and the basicity of solvents strongly influenced the linker conformation in the resultant MOFs, leading to the topology evolution. Such a solvent- and acid-assisted topology evolution represents a general approach that can be used with other tetratopic carboxylate linkers to realize structural diversity. The present work demonstrates an effective structure designing strategy by controlling synthetic conditions, which may prove to be powerful for customized synthesis of MOFs with specific structure and functionality.

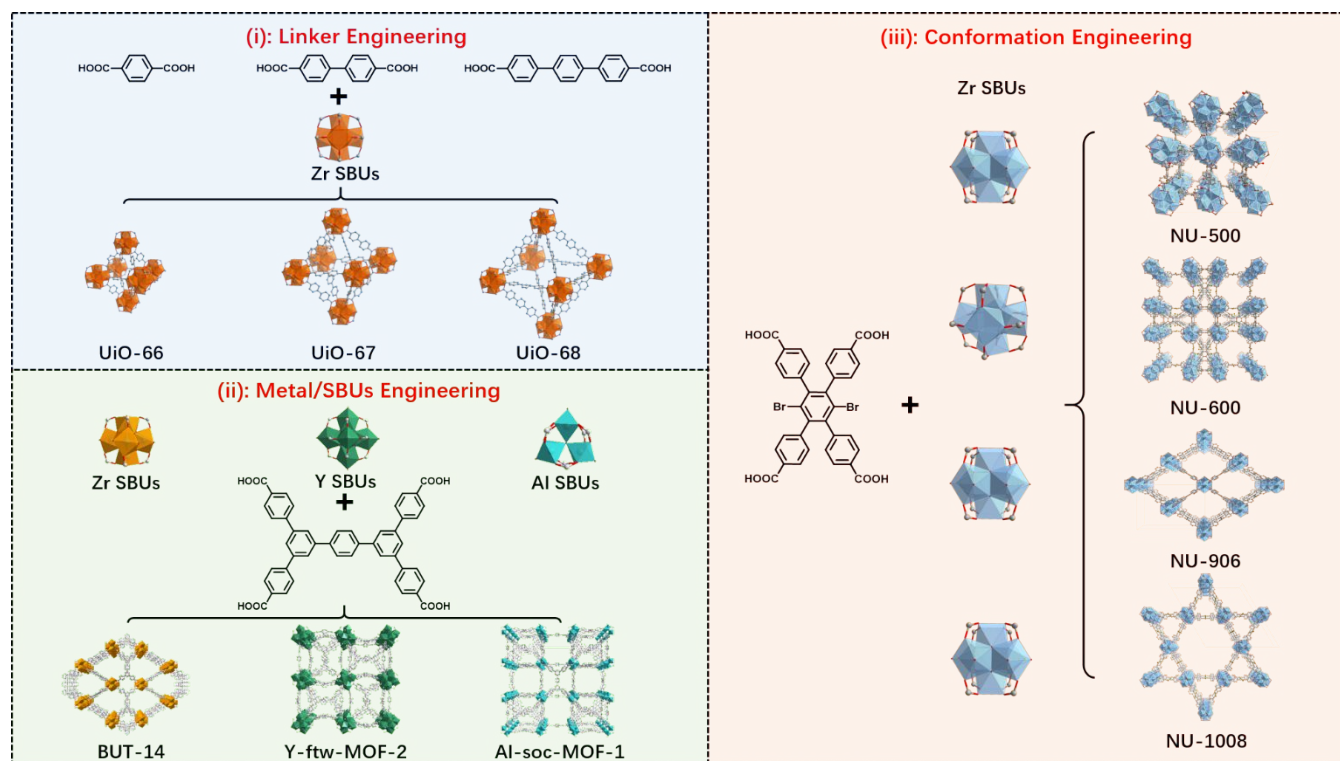


INTRODUCTION

Metal-organic frameworks (MOFs) are a category of hybrid porous materials built of inorganic metal ions/clusters and organic linkers through coordination bonds.¹⁻² Tunable structures of MOFs give rise to diversity of structures and functionalities, which allow them to be customized for a wide variety of important applications, including but not limited to gas storage and separation,³⁻⁴ luminescence based sensing and photonics⁵⁻⁶ as well as heterogeneous catalysis⁷⁻⁸. So far, some 100,000 MOF compounds have been reported,⁹ offering a large pool of functional materials for target-specific applications and devices.¹⁰ To make them ready for commercialization, directional synthesis of customized MOF structures signifies the next stage of the MOF development.¹¹

Assembly of various metal ions/clusters and organic linkers confer the diversity of MOFs. Three strategies have been commonly utilized for customized MOFs synthesis. As shown in Scheme 1, (i) Linker Engineering is a powerful way to

introduce specific properties or new functions to MOFs.¹²⁻¹⁶ For example, UiO-66, UiO-67 and UiO-68 possess the same topology with increased pore size as a result of increasing ligand length.¹⁷ The same strategy has been used to prepare MOF-74 series with large-pore apertures.¹⁴ Additionally, pre- and post-synthesis linker modification,^{16, 18, 19} and linker installation²⁰⁻²⁴ have also been proven to be useful approaches to achieve target-specific properties on resultant MOFs. (ii) Metal/SBUs Engineering (SBU: secondary building unit) is another strategy to create the structure diversity in MOFs.²⁵ Assembly of different SBUs with the same linker result in different underlying nets.²⁶⁻²⁷ For instance, the simplest and rigid ditopic terephthalic acid, H₂bdc, is the first organic linker adopted in MOF synthesis. It has been used to connect with several metal nodes, such as Zr, Zn, Al, Cr and Ti SBUs, to form UiO-66,¹⁷ MOF-5,²⁸⁻²⁹ MIL-53,³⁰ MIL-101³¹ and MIL-125³², to name a few. Varying structures, like BUT-14,³³ Y-ftw-MOF-2³⁴ and Al-soc-MOF-1³⁵, can be formed when Zr, Y and Al were used as the metal source and 3,3',5,5'-tetrakis(4-carboxyphenyl)-p-ter



Scheme 1. Schematic representation of the three strategies for customized MOF synthesis: (i) Linker Engineering, (ii) Metal/SBUs Engineering and (iii) Conformation Engineering.

phenyl was used as the organic linker (Scheme 1). Strategies mentioned above concentrate on the diversity of linkers and SBUs, which leads to a very rich MOF structural database. On the other hand, other structure-directing parameters also exist, such as molecular stretching and twisting of the linkers that often give rise to different conformations. They also play an important role in the topology of the final structures of MOFs. These parameters can be controlled by varying synthetic conditions, including solvent and acid modulator.³⁶⁻³⁷ This strategy is categorized as (iii) Linker Conformation Engineering (Scheme 1). A suitable combination of solvent and modulating chemical species can directly affect the conformation of linkers, resulting in different nets with the same linker and metal node.³⁸

Tetratopic carboxylates are good candidates of linkers to generate conformation-dependent topologies compared with tricarboxylic and dicarboxylic acid-based linkers. For example, as one of the most extensively studied linkers, tetrakis-(4-carboxyphenyl)porphyrin (H₄TCPP) has been reported to form several topologies with Zr₆ clusters,³⁹ where the underlying net is determined by the conformation of TCPP and the connectivity of Zr₆ cluster controlled by various synthetic conditions. In addition, as a useful strategy to influence the linker conformation, steric hindrance has been introduced into the linker backbone to control the nets of resulting MOFs.⁴⁰ Zhou and co-workers systematically studied a series of (4,8)-c Zr-tetracarboxylate-based MOFs by changing the substituents on different positions of the tetratopic carboxylate linkers.⁴¹ Tunable linker rotamers lead to three types of structures with

csq, **flu** and **scu** topologies underlying nets under controllable solvothermal conditions. These results indicate that rationally selecting the modulators and solvent serves an effective way in directing MOF structures. However, to this date, there is lack of works to systemically study the relationship between them.

In a recent report, Farha and co-workers studied solvent and acid effect on the topologies of resultant Zr-MOFs using 1,4-dibromo-2,3,5,6-tetrakis (4-carboxyphenyl) benzene (H₄TCPB-Br₂) as the linker.³⁸ Two kinds of solvents (N,N-dimethyl formamide, DMF; N,N-diethyl formamide, DEF) and two types of acid modulators (formic acid, FA; acetic acid, AA) were investigated. By precisely modulating the synthetic conditions, the connectivities of Zr₆ cluster and the conformations of the TCPB-Br₂ can be simultaneously controlled. As a result, four different topologies were obtained, i.e. a new 4,4,4,5-coordinated tetranodal net (NU-500), 4,6-c **she** (NU-600), 4,8-c **scu** (NU-906), and 4,8-c **csq** (NU-1008) as shown in Scheme 1.

Very recently, we have also prepared a series of Zr-MOFs HIAM-400X (HIAM = Hoffmann Institute of Advanced Materials, 40 = Zirconium, X = 0-4) using a similar tetracarboxylic acid linker.²¹ One **scu** net, same as NU-906, was obtained in DMF solvent with benzoic acid as the acid. An interesting question is would it be possible to attain other nets when different solvents and acids are utilized? To explore such possibilities and to understand how reaction conditions affect important structural parameters that govern topological evolution, such as linker conformation and SBU connectivity, we carried out a systematic study to

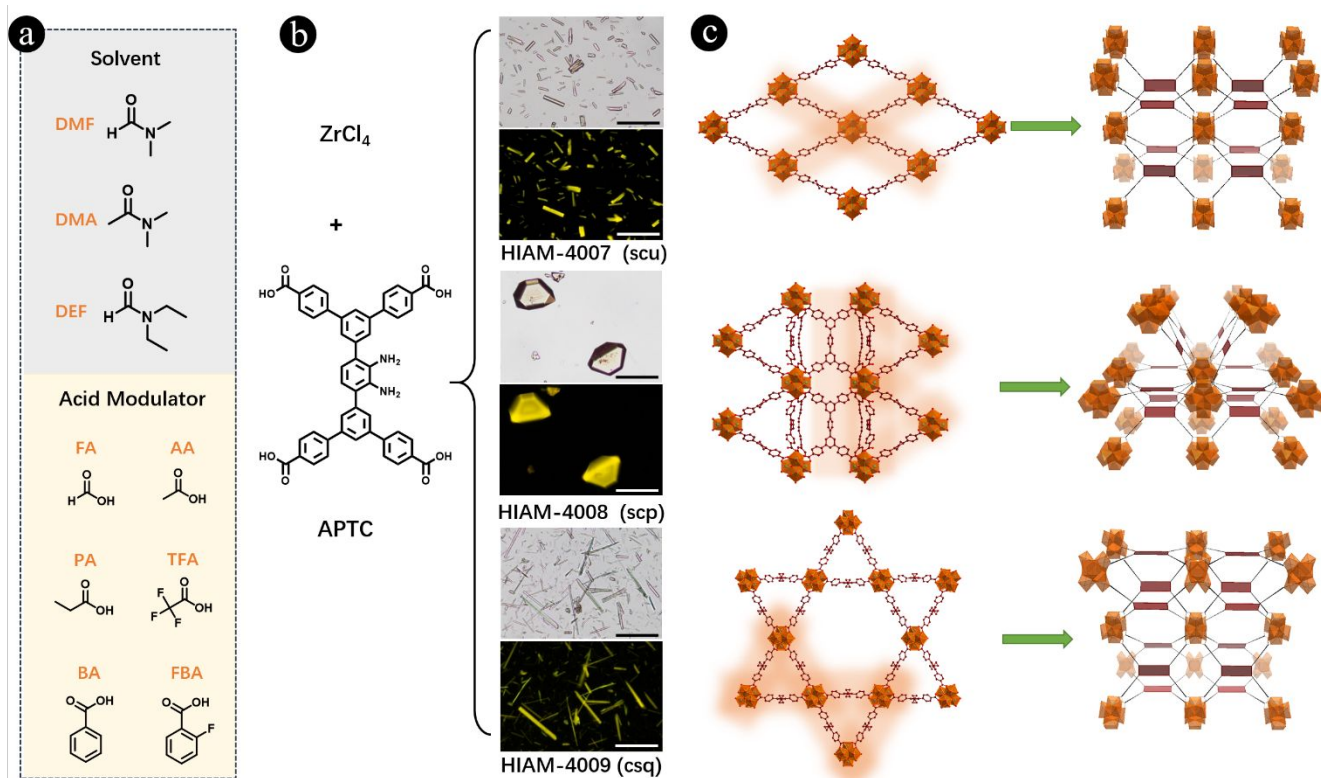


Figure 1. (a) The molecular structure of three solvents and six different acids modulator employed for MOFs synthesis; (b) schematic representation of the preparation and the single crystal images of HIAM-4007, HIAM-4008 and HIAM-4009 under daylight and 450 nm excitation (scale bar: 100 μ m); (c) the single crystal structure of HIAM-4007, HIAM-4008 and HIAM-4009 (Color scheme: C, brown; O, red; Zr, green. H and N atoms in the structures are omitted for clarity.).

synthesize a series of Zr-MOFs composed of the same tetracarboxylate linker under various combination of solvents and acids, and to evaluate the mechanism of topological evolution of MOFs formed under different reaction conditions.

RESULTS AND DISCUSSION

Solvent- and Acid-assisted Topology Evolution of Zr-Tetracarboxylate Frameworks. Based on the aforementioned considerations, we firstly designed and synthesized a linker, 5',5'''-(2,3-diaminophenyl)-bis((1,1':3',1''-terphenyl)-4,4''-dicarboxylic acid) (APTC), similar to that used in HIAM-400X (X = 0-4) via Suzuki reactions and followed hydrolysis under mild conditions as shown Supporting Information. Similar linkers have been utilized to prepare Zr-MOFs with **sqc** and **csq** topology under different solvothermal conditions.^{21, 42-43} To systematically study the effects of solvent and acid on the topology evolution of Zr-MOFs, three solvents, N,N-diethyl formamide (DEF), N,N-dimethyl acetamide (DMA) and N,N-dimethyl formamide (DMF), were selected along with six different acids, namely benzoic acid (BA), 2-fluorobenzoic acid (FBA), formic acid (FA), acetic acid (AA), propionic acid (PA) and trifluoroacetic acid (TFA) as modulators (see Figure 1a). To avoid temperature- and reaction time-induced structure diversity, the synthetic temperature was fixed at 120 $^{\circ}$ C, and the reaction time was fixed for 3 days. By various combinations of the selected solvents and acids, the reactions of $ZrCl_4$ (metal source) and APTC (linker) resulted in three structures: HIAM-4007 (**scu**), HIAM-4008 (with the new trinodal 4,4,12-c **scp**

net) and HIAM-4009 (**csq**)²⁰ as shown in Figure 1b-1c. The detailed synthesis conditions are listed in Table S1. These results indicate that the structures and topologies of the Zr-based MOFs can indeed be tuned through suitable choice of solvent and modulator.

Structural Analysis and Description of HIAM-4007, HIAM-4008 and HIAM-4009. Prismatic crystals of HIAM-4007 were obtained by solvothermal reaction of $ZrCl_4$ and APTC in DMF with benzoic acid served as the modulator, which was similar to the synthetic procedure for HIAM-4000. Single crystal X-ray diffraction (sc-XRD) analysis revealed that HIAM-4007 crystallized in orthorhombic crystal system with $Cmmm$ space group (Table S2). Each Zr_6O_8 cluster is coordinated by eight fully deprotonated APTC linkers and eight terminal H_2O/OH -groups. Each APTC is connected to four Zr_6 clusters, leading to a (4,8)-c **scu** net in HIAM-4007 (Figure 1c). These data give the overall formula of HIAM-4007 as $Zr_6O_4(OH)_8(H_2O)_4(APTC)_2$. Four types of one-dimensional (1D) open channels are formed, i.e. rhombic channels and hexagonal channels along a -axis, and two different rhombic channels along b - and c - axis (Figure S1). The permanent porosity of HIAM-4007 was examined by N_2 sorption isotherms at 77 K with the Brunauer-Emmett-Teller (BET) surface areas of 496.1 m^2/g and total pore volume of 0.206 cm^3/g (Figure S2).

The solvothermal reaction of $ZrCl_4$ and APTC linker using DEF as solvent and acetic acid as modulator yielded truncated octahedral crystals of HIAM-4008. The sc-XRD analysis indicated that HIAM-4008 crystallizes in tetragonal crystal

system with $I4_1/amd$ space group (Table S3). HIAM-4008 also possesses Zr_6O_8 cluster, but each Zr_6 cluster is coordinated by twelve APTC linkers and four terminal H_2O/OH^- groups, leading to a new trinodal (4,4,12)-c **scp** net in HIAM-4008 (Figure 1c and Figure S3). In this structure, eight APTCs are coordinated with Zr_6 cluster via bidentate carboxylate group. While the other four APTCs are disorder over two positions (50%-50%). The disordered APTC is monodentate to Zr_6 cluster (Figure S4). From a topological viewpoint, the connectivity of the Zr_6 node increases from 8 in HIAM-4007 to 12 in HIAM-4008 by changing solvent and acid, while all APTC linkers connect always four Zr_6O_8 clusters. The formula of HIAM-4008 thus is $Zr_6O_4(OH)_4(H_2O)_4(APTC)_3$. Three types of 1D open channels are formed, namely, triangle channels, trapezoid channels and rhombic channels along both a -axis and b -axis, while no open channels are formed along the c -axis (Figure S3). The BET surface areas and total pore volume are 1903.9 m^2/g and 0.687 cm^3/g for HIAM-4008, respectively (Figure S5).

Thinner and longer prismatic crystals of HIAM-4009 were obtained via the solvothermal reaction of $ZrCl_4$ and APTC linker in DEF with benzoic acid as the modulator. The prismatic single crystals of HIAM-4009 (**csq**) are not large enough for sc-XRD analysis. Topology of HIAM-4009 was determined by comparing the structures of HIAM-4009 and the similar Zr-MOF, PCN-808, with the overall formula of $Zr_6O_4(OH)_8(H_2O)_4(APTC)_2$.²¹ Each Zr_6 cluster in HIAM-4009 is coordinated by eight fully deprotonated APTC linkers and eight terminal H_2O/OH^- groups (Figure 1c). Each APTC is connected to four Zr_6 clusters to form a (4,8)-c **csq** topology in HIAM-4009, different from **scu** found for HIAM-4007. Two types of one-dimensional open channels are formed along c -axis, i.e., one triangle channel and one hexagonal channel (Figure S6). The corresponding BET surface areas and total pore volume are 1294.9 m^2/g and 0.759 cm^3/g for HIAM-4009, respectively (Figure S7). According to the N_2 sorption data, the pore size distributions based density functional theory (DFT) method indicated hierarchically porous structures with micropores at 14.1 Å, and mesopores at 26.6 Å for HIAM-4009 (Figure S7).

For Tetratopic carboxylic acid-based MOF, other topologies were also reported, such as (4, 12)-c **ftw**, (4,8)-c **scq** and (4,8)-c **flu**. However, we did not obtain these structures in our study, which might be contributed to the following facts: i) Zr_6 -based **ftw** net has strict demands on the linker size, i.e. aspect ratio;⁴⁴ ii) (4,8)-c **scq** net might be prepared after removing the two independent APTC from (4, 4, 12)-c **scp** net, as reported by Prof. Yang's group;⁴³ iii) **flu** net needs the linkers with tetrahedral conformation.⁴¹

Linker Conformation Analysis in Different MOFs. As mentioned earlier, molecular stretching and twisting commonly exist in MOF structures and often they determine the final topology of MOFs. In our work, no steric hindrance was introduced into the linker backbone, and amount of $ZrCl_4/APTC$ linker (23.3 mg/10 mg) and reaction temperature/time (120 °C/3 days) were all kept constant, while the type and amount of solvent and modulator were varied. In addition, all three structures (HIAM-4007, HIAM-4008 and HIAM-4009) are composed of the same Zr_6 clusters (SBUs).

Therefore, the conformations of the APTC linker played a dominating role in the final topology in these structures.

The conformations of the APTC linkers in the three Zr-MOFs are depicted in Figure 2. For the purpose of clarity, both amino groups on the phenyl ring are omitted. The linkers in (4,8)-c **scu** net of HIAM-4007 display only one crystallographic conformation (type I), with a C_{2h} symmetry. Both pairs of the adjacent phenyl arms rotate 43.3° in the same direction. In (4,8)-c **csq** net of HIAM-4009, the APTC linkers also display only one crystallographic conformation. Different from that in HIAM-4007, the linker here has a C_{2v} symmetry (type IV), in which two adjacent phenyl arms rotate away from each with the same angle of 49.6°. Interestingly, the linkers in HIAM-4008 display both crystallographic conformations (type II and type III) similar to type I and type IV. It is worth noting that only the APTC linkers displayed on the plane between a -axis and b -axis have the conformation with C_{2v} symmetry, in which with two adjacent phenyl arms rotate away from each with the same angle of 49.6°. The other type of APTC linkers possess the C_{2h} symmetry, in which both pairs of the adjacent phenyl arms rotate 44.5° in the same direction. Thus, the twisting of phenyl rings within APTC linker conformations determine the topologies in resulting HIAM-4007, HIAM-4008 and HIAM-4009.

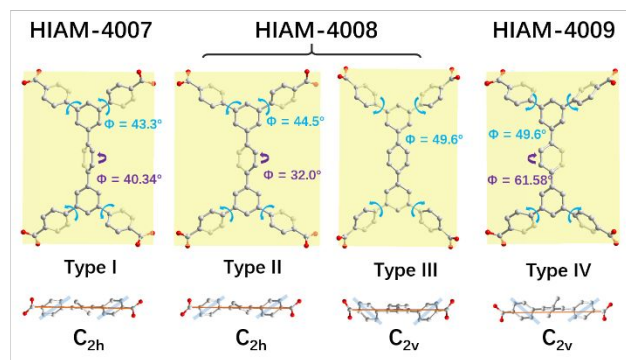


Figure 2. The twisting of the phenyl rings in the different conformations of APTC linker in HIAM-4007, HIAM-4008 and HIAM-4009.

Structure Effect on Photoluminescent Properties. As shown in Figure S8, similar photoluminescence, UV-vis absorption and TGA behaviors were observed for HIAM-4007, HIAM-4008 and HIAM-4009. However, due to varying linker conformations and packing in different nets, the interactions between linkers will be influence. As a result, different photoluminescence quantum yields (PLQYs) were recorded for these three MOFs. The PLQYs are 6.1%, 2.8% and 5.7% under 450 nm excitation for HIAM-4007, HIAM-4008 and HIAM-4009, respectively. The lowest PLQY for HIAM-4008 could be ascribed to the fact that (4,4,12)-c **scp** net with the highest linker density compared with (4,8)-c **scu** and **csq** nets, which will lead to the severest aggregation-cause luminescence quenching. In addition, from the single crystal analysis, organic linkers in (4,8)-c **csq** HIAM-4009 (Figure 1C, S1 and S4) possesses stronger π - π stacking interactions than (4,8)-c **scu** HIAM-

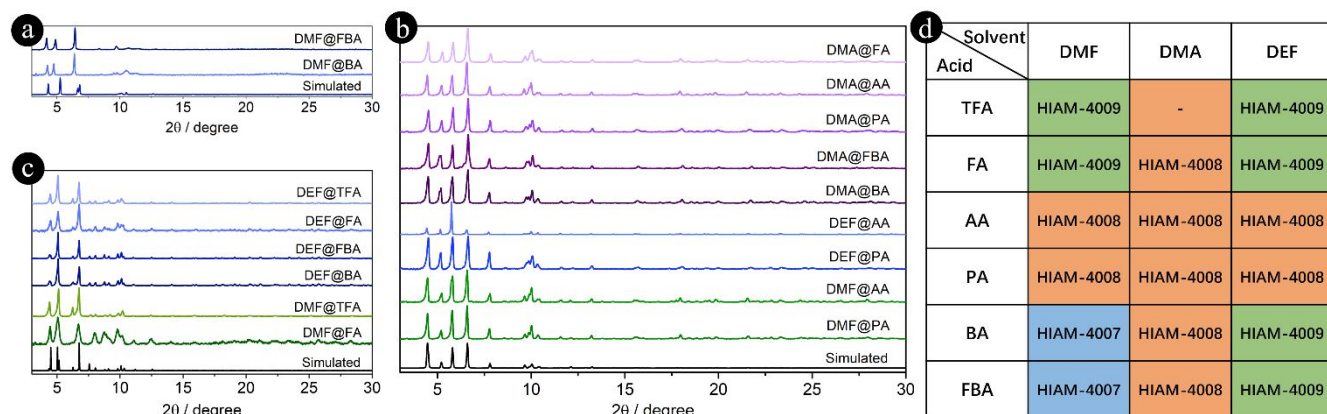


Figure 3. The PXRD patterns of HIAM-4007 (a), HIAM-4008(b) and HIAM-4009 (c) synthesized from different solvothermal conditions (d).

4007, which will result higher PLQY for HIAM-4007 than that of HIAM-4009. These results demonstrate that MOFs structures have significant effect on their photoluminescent properties, in which acid- and solvent-assisted topology evolution could be used as useful method to customized synthesis MOFs with highest performance.

Characterization of MOFs Synthesized using Different Solvents and Acids. As aforementioned, the linker conformation and consequently the topology of MOFs vary with different combinations of solvents and acids. Table S1 summarizes the details of such combinations using three types of solvents (DEF, DMA and DMF) and six acid modulators (BA, FBA, FA, AA, PA and TFA). The results show that adjusting the ratio of acid modulator made slight effort on the topology, while several exceptions were observed when much lower or higher concentration of acids was used (Table S1, Figure S9-S14). Therefore, only crystals obtained with mid-concentration of each acid modulator was further analyzed. Images of all crystal samples were summarized in Figures S6-8. The phase purities of HIAM-4007, HIAM-4008 and HIAM-4009 were confirmed by the excellent agreement between the experimental powder X-ray diffraction (PXRD) patterns and the simulated ones generated from the corresponding single crystal diffraction data.

In the case of HIAM-4007, as observed in Figure 3a and 3d, there are only two kinds of combinations that resulted to this topology. In both cases, DMF was used as solvent with BA or FBA as acid modulators. There are notable peak shifts in the PXRD patterns for both dried crystals, due to their structural flexibility. In the case of HIAM-4008, nine different combinations generated this topology (Figure 3b and 3d). Finally, six combinations succeeded in producing HIAM-4009. It was notable that highly crystalline samples were obtained either in DEF or with TFA/FA as acid modulators (Figure 3c and 3d). The PXRD analysis also suggests that combinations of DMF and FA generally resulted in less crystalline samples. Based on the data shown in Figure 3d, it is also clear that reactions with DMA as solvent yielded exclusively HIAM-4008, regardless of what acid was used, except TFA, which as modulator yielded almost no crystals, and adjusting its amount also made no effect. In the case of DMF, all three types of Zr-MOFs can be synthesized. HIAM-4007 was obtained when BA and FBA were used; HIAM-

4008 was prepared using AA and PA as the modulators; while HIAM-4009 was obtained when TFA and FA were utilized. However, in the case of DEF, only two types of Zr-MOFs could be achieved. Considering acid modulators, use of AA and PA only resulted in HIAM-4008. Variation of solvents had no effect on the MOF topology. HIAM-4007 only occurred when BA or FBA was employed as acid modulators and DMF as solvent.

All above results demonstrate that the selection of solvent and acid modulator directly affect the resulting linker conformation and MOF structure. The topology of the Zr-MOFs built on the same linker and identical Zr_6 cluster can be controlled by solvents and acid modulators.

Mechanism of Topology Evolution of Different MOFs. To understand the factors that contribute to various conformations of APTC in HIAM-4007,8,9, we investigated further possible mechanism of crystal formation. The results from the previous section demonstrate that the topology evolution from HIAM-4007 to HIAM-4009 was controlled solely by the choices of solvents and acids used in the synthesis, which directed to different linker conformations in the final crystal structures. It is well known that the pKa of an acid makes significant effect on the nucleation and crystal growth by competing with linkers for coordination sites on Zr_6 clusters to terminate the coordination process and to form Zr_6 nodes with lower connectivity.^{38-39, 45-46} Solvents with different physical and chemical properties also influence the nucleation and crystal growth processes by altering the solubility of the organic linkers and the degree of interaction with acids.⁴⁷ Therefore, we carried out a systematic comparison of the acidity of the modulating acids and the basicity of solvents to understand their effect on the topology evolution.

The pKa values of all the solvents and modulators used in this study are summarized in Table 1.⁴⁸⁻⁵¹ From the table, the pKa of modulators increases in the order of TFA, FBA, FA, BA, AA and PA. As has been observed, AA and PA leads to HIAM-4008 structure, which is a (4,4,12)-c **scp** underlying net. As reported previously, the modulator with higher pKa would lead to a weaker competition with linker for coordinating with Zr_6 cluster, thereby giving rise to higher connectivity of the metal nodes in the resulting MOFs.³⁸ Accordingly, in the case of AA and PA with highest pKa

values among the selected acid modulators, HIAM-4008 with fully connected nodes was obtained, regardless of which solvent was used. On the contrary, for the acid modulators with lower pKa values such as BA, FA, FBA and TFA, (4,8)-*cscu* and *esp* nets with lower connectivity were resulted in HIAM-4007 and HIAM-4009 with DEF or DMF employed as solvent.

Interestingly, FBA has a similar pKa to FA, indicating that the competitiveness of FA and FBA towards APTC linker for coordinating with Zr₆ node should be similar. But different structures were resulted in DMF. HIAM-4009 was obtained with FA, while HIAM-4007 was acquired with FBA. In HIAM-4007, a rhombic-shaped channel along the *c*-axis is observed, while two types of one-dimensional open channels are formed in HIAM-4009 along *c*-axis: triangle-shaped channel and hexagon-shaped channel (Figure S1 and S6). Notably, this additional smaller triangle-shaped channel is formed in HIAM-4009. Considering the steric hindrance of the two acids, FBA possesses a larger molecular size than FA. Thus it might be difficult for FBA to form small triangular channel to form HIAM-4009. Accordingly, a monotonous rhombic-shaped channel was formed in HIAM-4007. While the smaller sized FA gives rise to the coordination diversity in HIAM-4009, giving rise to two types of one-dimensional open channels.

Table 1. The pKa of acids and solvents used in this study.

acid	pKa	solvent	pKa
TFA	0.3	DMF	-0.70
FBA	3.6		
FA	3.7	DEF	-0.50
BA	4.2		
AA	4.8	DMA	0.10
PA	4.9		

Considering solvent effect, only one type of MOFs, namely HIAM-4008, was obtained in DMA, while all three types of MOFs could be synthesized in DMF, and two types of MOFs, HIAM-4008 and HIAM-4009, can be crystallized in DEF. Since the APTC linker dissolves completely in all three solvents, polarity of the solvents plays little role and thus, is not studied here. The basicity of the three solvents were considered. The basicity increases in the order of DMF, DEF and DMA. DMA shows the strongest basicity, which will weaken the competition of acid with linker for coordinating with the Zr₆ cluster, leading to the higher connectivity of Zr₆ cluster. The basicity of DEF was stronger than DMF but weaker than DMA, resulting in two topologies. With the weakest acids, AA and PA, HIAM-4008 with higher connectivity was formed using DEF as the solvent. With the increased acidity, the HIAM-4009 with lower connectivity was obtained. The synthetic process became extremely complicated when DMF was used as the solvent, which involved deprotonation of linkers, interaction between solvent and acid, and the competition between acid and linker for the coordinating with Zr₆ cluster. DMF has the lowest basicity, thereby the acid with different acidity will make a significant effect on the crystal nucleation and growth. As a result, three topologies were generated. All above results demonstrate that the solvents and acids controlled the topologies of MOFs

synergistically. Either solvent or acid plays an important role in determining the topologies of Zr-MOFs when their pKa values are extremely low or high.

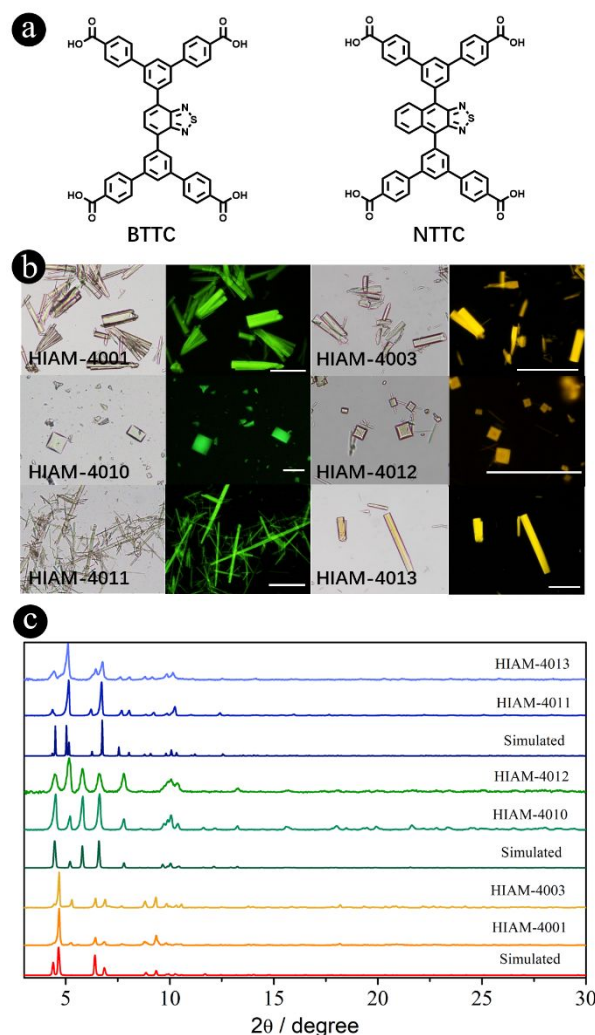


Figure 4. (a) The structures of tetracarboxylic acid ligand BTTc and NTTc used in the synthesis of HIAM-4001 and HIAM-4003. (b) The single crystal images of HIAM-4001, HIAM-4010, HIAM-4011, HIAM-4003, HIAM-4012 and HIAM-4013 under daylight (left) and 450 nm photoexcitation (right, scale bar: 100 μ m). (c) The PXRD patterns of HIAM-4001, HIAM-4010, HIAM-4011, HIAM-4003, HIAM-4012 and HIAM-4013 along with simulated ones.

Topology Control using different tetraprotic carboxylate linkers. As mentioned earlier, only one type topology was obtained for HIAM-4001 and HIAM-4003 in our previous study.²² In order to verify the proposed mechanism, we used the same linkers (BTTc and NTTc, see Figure 4a) but different solvents and acids to test out whether new types of Zr-MOFs can be obtained. AA and BA were adopted as the acid modulators, while DMA, DMF and DEF were selected as solvents. The synthesis detailed are provided in Supporting Information.

Six different Zr-MOFs were obtained, in which HIAM-4001 and HIAM-4003 were previously synthesized. BTTC linker led to two new types of Zr-MOFs. Truncated octahedron-shaped crystals of HIAM-4010 possess a (4,4,12)-c net, which is the same as we observed in HIAM-4008, while thinner and longer prismatic crystals of HIAM-4011 have a (4,8)-c **csq** net, which is the same as HIAM-4009. Similarly, for the linker NTTC, two new Zr-MOF structures were realized. Truncated octahedral crystals of HIAM-4012 and long prismatic crystals of HIAM-4013 possess the same topologies to those in HIAM-4008 and HIAM-4009 (Figure 4b). The phase purities of HIAM-4010 to HIAM-4013 were confirmed by the well agreed experimental PXRD patterns and the simulated ones generated from single crystal diffraction data of HIAM-4008 and HIAM-4009 (Figure 4c). The same reaction conditions as listed in Table S1 were used here, indicating that the proposed mechanism can be generalized for similar tetratopic carboxylate linkers to realize customized synthesis. More importantly, all three luminescent MOFs (LMOFs) made of the same linker exhibit very similar solid-state emission behavior, while the observed emission shifts were induced by the different packing of organic linkers in different nets (Figure S15). The similar effect on the PLQYs as we discussed for HIAM-4007 to HIAM-4009 was recorded for this series of LMOFs. For example, the highest PLQY is recorded for HIAM-4003 of 17.6% and the lowest PLQY is observed for HIAM-4012 of 8.8% with the highest linker density under 365 nm excitation. These results further indicated that acid- and solvent-assisted topology evolution could be used to customized synthesize MOFs with best performance.

Table S4 lists topologies of various tetratopic carboxylate-based Zr-MOFs obtained under different reaction conditions. For each linker, one or two topologies among **scu**, **csq**, **sqc** and **scp** are found. It should be noted that most of the MOFs adopt the same topologies as the HIAM-400X reported in the present work when the same solvent and acid were used, confirming that the proposed solvent- and acid-assisted topology evolution can be generalized. Note that introducing steric hindrance into the linker backbone or using linkers possessing very different molecular structure with the one we used in the present study will also influence linker conformation and lead to different topology of the resulting MOFs under similar synthesis conditions.

CONCLUSION

In conclusion, a systematic investigation has been conducted to evaluate topology evolution in Zr-MOFs directed by synthetic conditions. Combination of three solvents and six acids yielded three different topologies of Zr-MOFs using only the same Zr_6 SBU and tetratopic carboxylate linker. The different structures show significant influence on the photoluminescence quantum yield of resultant MOFs. Further experiments revealed that the basicity of solvents and the acidity of acids affected the structure of MOFs directly by modulating the protonation process of the organic linker and competition between the acid and linkers for coordination sites of the Zr_6 clusters. Rational selection of acid and solvent is a key factor in directing MOF structures. This principle

applies well to other tetratopic carboxylate linkers and represents a general approach for solvent- and acid-assisted topological evolution in Zr-MOFs. The current study may be helpful in establishing guideline for the customized synthesis of MOFs for target-specific applications and enhanced performances.

ASSOCIATED CONTENT

Supporting Information.

The Supporting Information is available free of charge on the ACS Publications website.

Materials synthesis, characterizations, tables for the single crystal data, and other additional information.

Crystallographic data for HIAM-4007 and HIAM-4008 with CCDC number 2129023 and 2129024(CIF).

AUTHOR INFORMATION

Corresponding Author

Xiao-Yuan Liu - Hoffmann Institute of Advanced Materials, Shenzhen Polytechnic, 7098 Liuxian Blvd, Nanshan District, Shenzhen, 518055, P.R. China; orcid.org/0000-0003-2400-8085; Email: liuxiaoyuan1989@szpt.edu.cn

Jing Li - Department of Chemistry and Chemical Biology, Rutgers University, 123 Bevier Road, Piscataway, New Jersey 08854, United States; Hoffmann Institute of Advanced Materials, Shenzhen Polytechnic, 7098 Liuxian Blvd, Nanshan District, Shenzhen, 518055, P.R. China; orcid.org/0000-0001-7792-4322; Email: jingli@rutgers.edu

Authors

Hai-Lun Xia - Hoffmann Institute of Advanced Materials, Shenzhen Polytechnic, 7098 Liuxian Blvd, Nanshan District, Shenzhen, 518055, P.R. China

Kang Zhou - Hoffmann Institute of Advanced Materials, Shenzhen Polytechnic, 7098 Liuxian Blvd, Nanshan District, Shenzhen, 518055, P.R. China

Liang Yu - Hoffmann Institute of Advanced Materials, Shenzhen Polytechnic, 7098 Liuxian Blvd, Nanshan District, Shenzhen, 518055, P.R. China

Hao Wang - Hoffmann Institute of Advanced Materials, Shenzhen Polytechnic, 7098 Liuxian Blvd, Nanshan District, Shenzhen, 518055, P.R. China

Davide M. Proserpio - Dipartimento di Chimica, Università degli Studi di Milano, Milano 20133, Italy; orcid.org/0000-0001-6597-9406.

Notes

The authors declare no competing financial interests.

ACKNOWLEDGMENT

H.-L. Xia gratefully acknowledge the funding support from Shenzhen Polytechnic (6021330018K). X.-Y. Liu acknowledges the financial support from start-up funding for Shenzhen High-Caliber Personnel of Shenzhen Polytechnic (6022310053K), Shenzhen Science and Technology Program (RCBS20200714114941230) and Guangdong Basic and Applied Basic Research Foundation (2020A1515110420).

REFERENCES

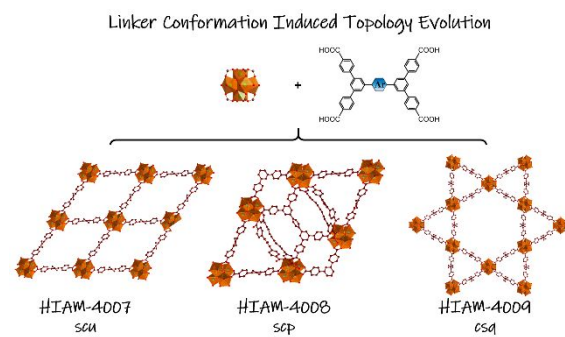
1. Furukawa, H.; Cordova, K. E.; O'Keeffe, M.; Yaghi, O. M.,

- The chemistry and applications of metal-organic frameworks. *Science* **2013**, *341* (6149), 1230444.
2. Feng, L.; Pang, J.; She, P.; Li, J.-L.; Qin, J.-S.; Du, D.-Y.; Zhou, H.-C., Metal-Organic Frameworks Based on Group 3 and 4 Metals. *Adv. Mater.* **2020**, *32* (44), 2004414.
3. Qian, Q.; Asinger, P. A.; Lee, M. J.; Han, G.; Mizrahi Rodriguez, K.; Lin, S.; Benedetti, F. M.; Wu, A. X.; Chi, W. S.; Smith, Z. P., MOF-Based Membranes for Gas Separations. *Chem. Rev.* **2020**, *120* (16), 8161-8266.
4. Adil, K.; Belmabkhout, Y.; Pillai, R. S.; Cadiau, A.; Bhatt, P. M.; Assen, A. H.; Maurin, G.; Eddaoudi, M., Gas/vapour separation using ultra-microporous metal-organic frameworks: insights into the structure/separation relationship. *Chem. Soc. Rev.* **2017**, *46* (11), 3402-3430.
5. Cui, Y.; Yue, Y.; Qian, G.; Chen, B., Luminescent Functional Metal-Organic Frameworks. *Chem. Rev.* **2012**, *112* (2), 1126-1162.
6. Lustig, W. P.; Mukherjee, S.; Rudd, N. D.; Desai, A. V.; Li, J.; Ghosh, S. K., Metal-organic frameworks: functional luminescent and photonic materials for sensing applications. *Chem. Soc. Rev.* **2017**, *46* (11), 3242-3285.
7. Chughtai, A. H.; Ahmad, N.; Younus, H. A.; Laypkov, A.; Verpoort, F., Metal-organic frameworks: versatile heterogeneous catalysts for efficient catalytic organic transformations. *Chem. Soc. Rev.* **2015**, *44* (19), 6804-6849.
8. Bavykina, A.; Kolobov, N.; Khan, I. S.; Bau, J. A.; Ramirez, A.; Gascon, J., Metal-Organic Frameworks in Heterogeneous Catalysis: Recent Progress, New Trends, and Future Perspectives. *Chem. Rev.* **2020**, *120* (16), 8468-8535.
9. Daglar, H.; Keskin, S., Recent advances, opportunities, and challenges in high-throughput computational screening of MOFs for gas separations. *Coord. Chem. Rev.* **2020**, *422*, 213470.
10. Liang, B.; Li, B.; Li, Z.; Chen, B., Progress in Multifunctional Metal-Organic Frameworks/Polymers Hybrid Membranes. *Chem. Eur. J.* **2021**, *27* (51), 12940-12952.
11. Bosch, M.; Yuan, S.; Rutledge, W.; Zhou, H. C., Stepwise Synthesis of Metal-Organic Frameworks. *Acc. Chem. Res.* **2017**, *50* (4), 857-865.
12. Banerjee, R.; Phan, A.; Wang, B.; Knobler, C.; Furukawa, H.; O'Keeffe, M.; Yaghi Omar, M., High-Throughput Synthesis of Zeolitic Imidazolate Frameworks and Application to CO₂ Capture. *Science* **2008**, *319* (5865), 939-943.
13. Deng, H.; Doonan Christian, J.; Furukawa, H.; Ferreira Ricardo, B.; Towne, J.; Knobler Carolyn, B.; Wang, B.; Yaghi Omar, M., Multiple Functional Groups of Varying Ratios in Metal-Organic Frameworks. *Science* **2010**, *327* (5967), 846-850.
14. Deng, H.; Grunder, S.; Cordova, K. E.; Valente, C.; Furukawa, H.; Hmadeh, M.; Gandara, F.; Whalley, A. C.; Liu, Z.; Asahina, S.; Kazumori, H.; O'Keeffe, M.; Terasaki, O.; Stoddart, J. F.; Yaghi, O. M., Large-pore apertures in a series of metal-organic frameworks. *Science* **2012**, *336* (6084), 1018-1023.
15. Lu, W.; Wei, Z.; Gu, Z.-Y.; Liu, T.-F.; Park, J.; Park, J.; Tian, J.; Zhang, M.; Zhang, Q.; Gentle Iii, T.; Bosch, M.; Zhou, H.-C., Tuning the structure and function of metal-organic frameworks via linker design. *Chem. Soc. Rev.* **2014**, *43* (16), 5561-5593.
16. Ali Akbar Razavi, S.; Morsali, A., Linker functionalized metal-organic frameworks. *Coord. Chem. Rev.* **2019**, *399*, 213023.
17. Cavka, J. H.; Jakobsen, S.; Olsbye, U.; Guillou, N.; Lamberti, C.; Bordiga, S.; Lillerud, K. P., A New Zirconium Inorganic Building Brick Forming Metal Organic Frameworks with Exceptional Stability. *J. Am. Chem. Soc.* **2008**, *130* (42), 13850-13851.
18. Wu, S.; Ren, D.; Zhou, K.; Xia, H. L.; Liu, X. Y.; Wang, X.; Li, J., Linker Engineering toward Full-Color Emission of UiO-68 Type Metal-Organic Frameworks. *J. Am. Chem. Soc.* **2021**, *143* (28), 10547-10552.
19. Mandal, S.; Natarajan, S.; Mani, P.; Pankajakshan, A., Post-Synthetic Modification of Metal-Organic Frameworks Toward Applications. *Adv. Funct. Mater.* **2021**, *31* (4), 2006291.
20. Yuan, S.; Lu, W.; Chen, Y.-P.; Zhang, Q.; Liu, T.-F.; Feng, D.; Wang, X.; Qin, J.; Zhou, H.-C., Sequential Linker Installation: Precise Placement of Functional Groups in Multivariate Metal-Organic Frameworks. *J. Am. Chem. Soc.* **2015**, *137* (9), 3177-3180.
21. Pang, J.; Di, Z.; Qin, J. S.; Yuan, S.; Lollar, C. T.; Li, J.; Zhang, P.; Wu, M.; Yuan, D.; Hong, M.; Zhou, H. C., Precisely Embedding Active Sites into a Mesoporous Zr-Framework through Linker Installation for High-Efficiency Photocatalysis. *J. Am. Chem. Soc.* **2020**, *142* (35), 15020-15026.
22. Ren, D.; Xia, H.-L.; Zhou, K.; Wu, S.; Liu, X.-Y.; Wang, X.; Li, J., Tuning and Directing Energy Transfer in the Whole Visible Spectrum through Linker Installation in Metal-Organic Frameworks. *Angew. Chem. Int. Ed.* **2021**, *60* (47), 25048-25054.
23. Dolgoplova, E. A.; Ejegbavwo, O. A.; Martin, C. R.; Smith, M. D.; Setyawan, W.; Karakalos, S. G.; Henager, C. H.; zur Loye, H.-C.; Shustova, N. B., Multifaceted Modularity: A Key for Stepwise Building of Hierarchical Complexity in Actinide Metal-Organic Frameworks. *J. Am. Chem. Soc.* **2017**, *139* (46), 16852-16861.
24. Han, G.; Wu, S.; Zhou, K.; Xia, H.-L.; Liu, X.-Y.; Li, J., Full-Color Emission in Multicomponent Metal-Organic Frameworks via Linker Installation. *Inorg. Chem.* **2022**, *61*(8), 3363-3367.
25. Eddaoudi, M.; Moler, D. B.; Li, H.; Chen, B.; Reineke, T. M.; O'Keeffe, M.; Yaghi, O. M., Modular Chemistry: Secondary Building Units as a Basis for the Design of Highly Porous and Robust Metal-Organic Carboxylate Frameworks. *Acc. Chem. Res.* **2001**, *34* (4), 319-330.
26. Alexandrov, E. V.; Blatov, V. A.; Kochetkov, A. V.; Proserpio, D. M., Underlying nets in three-periodic coordination polymers: topology, taxonomy and prediction from a computer-aided analysis of the Cambridge Structural Database. *CrystEngComm* **2011**, *13* (12), 3947-3958.
27. Blatov, V. A.; Shevchenko, A. P.; Proserpio, D. M., Applied Topological Analysis of Crystal Structures with the Program Package ToposPro. *Cryst. Growth Des.* **2014**, *14* (7), 3576-3586.
28. Li, H.; Eddaoudi, M.; O'Keeffe, M.; Yaghi, O. M., Design and synthesis of an exceptionally stable and highly porous metal-organic framework. *Nature* **1999**, *402* (6759), 276-279.
29. Eddaoudi, M.; Kim, J.; Rosi, N.; Vodak, D.; Wachter, J.; O'Keeffe, M.; Yaghi Omar, M., Systematic Design of Pore Size and Functionality in Isorecticular MOFs and Their Application in Methane Storage. *Science* **2002**, *295* (5554), 469-472.
30. Loiseau, T.; Serre, C.; Huguenard, C.; Fink, G.; Taulelle, F.; Henry, M.; Bataille, T.; Férey, G., A rationale for the large breathing of the porous aluminum terephthalate (MIL-53) upon hydration. *Chem. Eur. J.* **2004**, *10* (6), 1373-1382.
31. Férey, G.; Mellot-Draznieks, C.; Serre, C.; Millange, F.; Dautour, J.; Surblé, S.; Margiolaki, I., A Chromium Terephthalate-Based Solid with Unusually Large Pore Volumes and Surface Area. *Science* **2005**, *309* (5743), 2040-2042.
32. Dan-Hardi, M.; Serre, C.; Frot, T.; Rozes, L.; Maurin, G.; Sanchez, C.; Férey, G., A New Photoactive Crystalline Highly Porous Titanium(IV) Dicarboxylate. *J. Am. Chem. Soc.* **2009**, *131* (31), 10857-10859.
33. Wang, B.; Yang, Q.; Guo, C.; Sun, Y.; Xie, L. H.; Li, J. R., Stable Zr(IV)-Based Metal-Organic Frameworks with

1 Predesigned Functionalized Ligands for Highly Selective
 2 Detection of Fe(III) Ions in Water. *ACS Appl. Mater. Interfaces*
 3 **2017**, *9* (11), 10286-10295.
 4 34. Luebke, R.; Belmabkhout, Y.; Weselinski, L. J.; Cairns, A. J.;
 5 Alkordi, M.; Norton, G.; Wojtas, L.; Adil, K.; Eddaoudi, M.,
 6 Versatile rare earth hexanuclear clusters for the design and
 7 synthesis of highly-connected ftw-MOFs. *Chem. Sci.* **2015**, *6* (7),
 8 4095-4102.
 9 35. Alezi, D.; Belmabkhout, Y.; Suyetin, M.; Bhatt, P. M.;
 10 Weselinski, L. J.; Solovyeva, V.; Adil, K.; Spanopoulos, I.;
 11 Trikalitis, P. N.; Emwas, A. H.; Eddaoudi, M., MOF Crystal
 12 Chemistry Paving the Way to Gas Storage Needs: Aluminum-
 13 Based soc-MOF for CH₄, O₂, and CO₂ Storage. *J Am Chem Soc*
 14 **2015**, *137* (41), 13308-13318.
 15 36. Ma, J.; Tran, L. D.; Matzger, A. J., Toward Topology
 16 Prediction in Zr-Based Microporous Coordination Polymers: The
 17 Role of Linker Geometry and Flexibility. *Cryst. Growth Des.*
 18 **2016**, *16* (7), 4148-4153.
 19 37. Schneemann, A.; Bon, V.; Schwedler, I.; Senkowska, I.;
 20 Kaskel, S.; Fischer, R. A., Flexible metal-organic frameworks.
 21 *Chem. Soc. Rev.* **2014**, *43* (16), 6062-6096.
 22 38. Chen, Y.; Zhang, X.; Mian, M. R.; Son, F. A.; Zhang, K.; Cao,
 23 R.; Chen, Z.; Lee, S. J.; Idrees, K. B.; Goetjen, T. A.; Lyu, J.; Li,
 24 P.; Xia, Q.; Li, Z.; Hupp, J. T.; Islamoglu, T.; Napolitano, A.;
 25 Peterson, G. W.; Farha, O. K., Structural Diversity of Zirconium
 26 Metal-Organic Frameworks and Effect on Adsorption of Toxic
 27 Chemicals. *J. Am. Chem. Soc.* **2020**, *142* (51), 21428-21438.
 28 39. Chen, Z.; Hanna, S. L.; Redfern, L. R.; Alezi, D.; Islamoglu,
 29 T.; Farha, O. K., Reticular chemistry in the rational synthesis of
 30 functional zirconium cluster-based MOFs. *Coord. Chem. Rev.*
 31 **2019**, *386*, 32-49.
 32 40. Wang, B.; Lv, X. L.; Feng, D.; Xie, L. H.; Zhang, J.; Li, M.;
 33 Xie, Y.; Li, J. R.; Zhou, H. C., Highly Stable Zr(IV)-Based Metal-
 34 Organic Frameworks for the Detection and Removal of
 35 Antibiotics and Organic Explosives in Water. *J. Am. Chem. Soc.*
 36 **2016**, *138* (19), 6204-6216.
 37 41. Pang, J.; Yuan, S.; Qin, J.; Liu, C.; Lollar, C.; Wu, M.; Yuan,
 38 D.; Zhou, H. C.; Hong, M., Control the Structure of Zr-
 39 Tetracarboxylate Frameworks through Steric Tuning. *J. Am.*
 40 *Chem. Soc.* **2017**, *139* (46), 16939-16945.
 41 42. Wang, B.; Yang, Q.; Guo, C.; Sun, Y.; Xie, L. H.; Li, J. R.,
 42 Stable Zr(IV)-Based Metal-Organic Frameworks with
 43 Predesigned Functionalized Ligands for Highly Selective
 44 Detection of Fe(III) Ions in Water. *ACS Appl. Mater. Interfaces*
 45 **2017**, *9* (11), 10286-10295.
 46 43. Carter, J. H.; Han, X.; Moreau, F. Y.; da Silva, I.; Nevin, A.;
 47 Godfrey, H. G. W.; Tang, C. C.; Yang, S.; Schroder, M.,
 48 Exceptional Adsorption and Binding of Sulfur Dioxide in a
 49 Robust Zirconium-Based Metal-Organic Framework. *J. Am.*
 50 *Chem. Soc.* **2018**, *140* (46), 15564-15567.
 51 44. Wang, H.; Dong, X.; Colombo, V.; Wang, Q.; Liu, Y.; Liu,
 52 W.; Wang, X.-L.; Huang, X.-Y.; Proserpio, D. M.; Sironi, A.;
 53 Han, Y.; Li, J., Tailor-Made Microporous Metal-Organic
 54 Frameworks for the Full Separation of Propane from Propylene
 55 Through Selective Size Exclusion. *Adv. Mater.* **2018**, *30* (49),
 56 1805088.
 57 45. Schaate, A.; Roy, P.; Godt, A.; Lippke, J.; Waltz, F.;
 58 Wiebcke, M.; Behrens, P., Modulated Synthesis of Zr-Based
 59 Metal-Organic Frameworks: From Nano to Single Crystals.
 60 *Chem. Eur. J.* **2011**, *17* (24), 6643-6651.
 46. Wißmann, G.; Schaate, A.; Lilienthal, S.; Bremer, I.;
 Schneider, A. M.; Behrens, P., Modulated synthesis of Zr-
 fumarate MOF. *Microporous and Mesoporous Materials* **2012**,
152, 64-70.

47. Wasson, M. C.; Lyu, J.; Islamoglu, T.; Farha, O. K., Linker
 Competition within a Metal-Organic Framework for Topological
 Insights. *Inorg. Chem.* **2019**, *58* (2), 1513-1517.
 48. Hu, Z.; Wang, Y.; Zhao, D., The chemistry and applications
 of hafnium and cerium(IV) metal-organic frameworks. *Chem.*
Soc. Rev. **2021**, *50*, 4629-4683.
 49. Chun, A. Y.; Yunxiao, L.; Ashok, S.; Seol, E.; Park, S.,
 Elucidation of toxicity of organic acids inhibiting growth of
 Escherichia coli W. *Biotechnol. Bioproc. E* **2014**, *19* (5), 858-
 865.
 50. Pytela, O.; Prusek, O., Chemometric Analysis of Substituent
 Effects. XII. Application of Relationship Between 2- and 4-
 Substitution of Benzene Ring to Study ortho Effect in Selected
 Compounds with Different Reaction Centres. *Collect. Czech.*
Chem. Commun. **1999**, *64*, 1617-1628.
 51. Adelman, R. L., Studies on the Base Strengths of N,N-
 Disubstituted Amides. *J. Org. Chem.* **1964**, *29* (7), 1837-1844.

Table of Content



In the present work, we carried out a methodical study on the topology evolution in zirconium-tetracarboxylate frameworks directed by solvothermal conditions with various combinations of solvents and acids. The results revealed that the acidity of acids and the basicity of solvents influenced the linker conformations, leading to the topology evolution. Such a solvent- and acid-assisted topology evolution represents a general approach that can be used with other tetra-topic carboxylate linkers to realize structural diversity.

Supporting Information

Customized Synthesis: Solvent- and Acid-Assisted Topology Evolution Zirconium-Tetracarboxylate Frameworks

Hai-Lun Xia,^[a] Kang Zhou,^[a] Liang Yu,^[a] Hao Wang,^[a] Xiao-Yuan Liu,^{*,[a]} Davide M.

Proserpio,^[b] Jing Li^{*,[c],[a]}

^[a] Hoffmann Institute of Advanced Materials, Shenzhen Polytechnic, 7098 Liuxian Blvd, Nanshan District, Shenzhen, 518055, P.R. China

^[b] Dipartimento di Chimica, Università degli Studi di Milano, Milano 20133, Italy

^[c] Department of Chemistry and Chemical Biology, Rutgers University, 123 Bevier Road, Piscataway, New Jersey 08854, United States

* To whom correspondence should be addressed: liuxiaoyuan1989@szpt.edu.cn, jingli@rutgers.edu

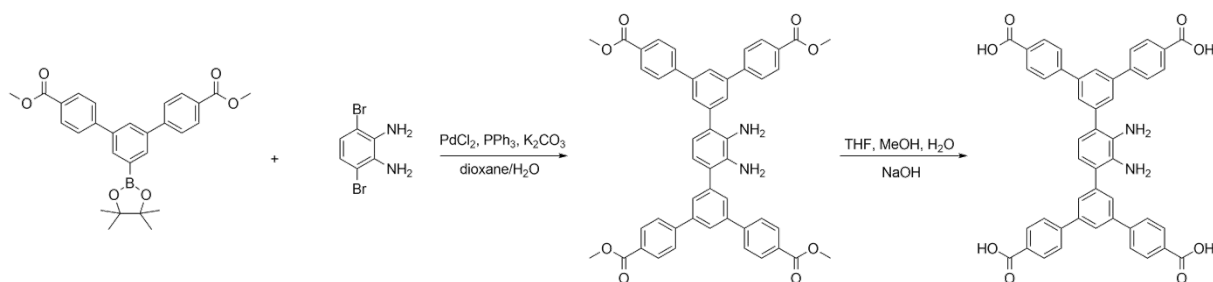
Chemicals

Dimethyl 5'-(4,4,5,5-tetramethyl-1,3,2-dioxaborolan-2-yl)-[1,1':3',1''-terphenyl]-4,4''-dicarboxylate and 3,6-dibromobenzene-1,2-diamine were purchased from Jilin Chinese Academy of Science-Yanshen Technology Co., Ltd. Other reagents and chemicals including benzoic acid (BA, 99.5%), 2-fluorobenzoic acid (FBA, 98.0%), formic acid (FA, 99.0%), acetic acid (AA, 99.8%), propionic acid (PA, 99.5%), trifluoroacetic acid (TFA, 99.0%), N, N-diethyl formamide (DEF, 99.0%), N, N-dimethyl acetamide (DMA, 99.0%) and N, N-dimethyl formamide (DMF, 99.5%) were purchased from Shanghai Aladdin Biochemical Technology Co., Ltd.. 5',5'''-(benzo[c][1,2,5]thiadiazole-4,7-diyl)bis(([1,1':3',1''-terphenyl]-4,4''-dicarboxylic acid)) (BTTC) and 5',5'''-(naphtho[2,3-c][1,2,5]thiadiazole-4,9-diyl)bis(([1,1':3',1''-terphenyl]-4,4''-dicarboxylic acid)) (NTTC) were synthesized according to previous work.¹

Characterization

Nuclear magnetic resonance (NMR) data was obtained using 400 MHz JEOL JNM-ECZ400S. Powder X-ray diffraction (PXRD) patterns of all MOFs were measured using Bruker D8 Advance X-ray diffractometer with Cu K α radiation. Single crystal X-ray diffraction data were collected at 100 K on a Bruker D8 Venture diffractometer with graphite monochromated Ga K α radiation ($\lambda = 1.34139 \text{ \AA}$). The photoluminescent spectra were recorded on FLS1000 spectrofluorometer (Edinburgh Instruments). The UV-vis spectra were measured on Shimadzu UV-3600 spectrophotometer. The thermogravimetric data was collected using TGA 550 (TA Instruments) analyzer and the samples were heated from room temperature to 600°C at a ramp rate of 10°C / min.

Synthesis



Synthesis of tetramethyl 5',5'''-(2,3-diamino-1,4-phenylene)bis([1,1':3',1''-terphenyl]-4,4''-dicarboxylate)

Dimethyl 5'-(4,4,5,5-tetramethyl-1,3,2-dioxaborolan-2-yl)-[1,1':3',1''-terphenyl]-4,4''-dicarboxylate (4.4 mmol, 2.07 g), 3,6-dibromobenzene-1,2-diamine (2.0 mmol, 0.53 g), PdCl₂ (0.4 mmol, 0.07 g), PPh₃ (0.8 mmol, 0.21 g) and K₂CO₃ (16.0 mmol, 2.20 g) were added in a mixture solution of 120 mL dioxane and 30 mL water. The mixture solution was degassed four times and heated to reflux at 105 °C for 6 h under nitrogen atmosphere. After cooling to room temperature, the solvent was removed under reduced pressure. Then 100 mL DI water was added and the crude product was obtained after filtration. After purification by column chromatography, tetramethyl 5',5'''-(2,3-diamino-1,4-phenylene)bis([1,1':3',1''-terphenyl]-4,4''-dicarboxylate) was obtained as a pale yellow solid (0.98 g, 61.2%). ¹H NMR (400 MHz, CDCl₃) δ ppm 8.15 (8H), 7.87 (2H), 7.78 (8H), 7.75 (4H), 6.93 (2H), 3.95 (12H).

Synthesis of 5',5'''-(2,3-diamino-1,4-phenylene)bis([1,1':3',1''-terphenyl]-4,4''-dicarboxylic acid) (APTC)

Tetramethyl 5',5'''-(2,3-diamino-1,4-phenylene)bis([1,1':3',1''-terphenyl]-4,4''-dicarboxylate) (2.0 mmol, 1.59 g) was added to a mixture solution of 25 mL CH₃OH, 50 mL THF and 50 mL water with 4.0 g NaOH. The reaction solution was heated to reflux at 80 °C overnight. After cooling to room temperature, the organic solvent was removed under reduced pressure and the

resulted aqueous was filtered. Then the filtrate was neutralized using 2M HCl to obtain the precipitate, which was filtered to offer the final product as a brown solid (1.45 g, 98.0%). ¹H NMR (400 MHz, DMSO-*d*₆) δ ppm 8.05 (14H), 8.00 (4H), 7.98 (2H), 7.81 (4H) ppm.

Synthesis of HIAM-4007, HIAM-4001 and HIAM-4003

23.3 mg ZrCl₄, 10 mg APTC, 700 mg benzoic acid and 3 mL DMF were added in a 5 mL vial. The mixture was heated in a 120 °C oven for 3 days. After cooling down to room temperature, the pale yellow crystals of HIAM-4007 were obtained. HIAM-4001 and HIAM-4003 were synthesized using BTTC and NTTC as organic linkers based on the same method as HIAM-4007.

Synthesis of HIAM-4008, HIAM-4010, and HIAM-4012

23.3 mg ZrCl₄, 10 mg APTC, 1.25 mL acetic acid and 1.5 mL DEF were added in a 5 mL vial. The mixture was heated in a 120 °C oven for 3 days. After cooling down to room temperature, the pale yellow crystals of HIAM-4008 were obtained. HIAM-4010 was synthesized using BTTC in 3 mL DMA with 700 mg benzoic acid, and other conditions are the same with the synthesis of HIAM-4008. HIAM-4012 was synthesized using NTTC as organic linkers based on the same method as HIAM-4008.

Synthesis of HIAM-4009, HIAM-4011, and HIAM-4013

23.3 mg ZrCl₄, 10 mg APTC, 700 mg benzoic acid and 3 mL DEF were added in a 5 mL vial. The mixture was heated in a 120 °C oven for 3 days. After cooling down to room temperature, the pale yellow crystals of HIAM-4009 were obtained. HIAM-4011 and HIAM-4013 were synthesized using BTTC and NTTC as organic linkers based on the same method as HIAM-4009.

HIAM-4007, HIAM-4008 and HIAM-4009 were synthesized in different kinds of solvent and acids were summarized in Table S1.

Table S1. The synthesis conditions for HIAM-4007, HIAM-4008 and HIAM-4009.

Amount of ZrCl ₄ (mg)	Amount of linker (mg)	Acid (mL or mg)	Solvent (mL)	Solvothermal conditions	Crystal type	Crystal size
23.3	10	0.2 mL FA	2.0 mL DMF	120 °C, 3 days	HIAM-4009	Powder
		0.5 mL FA			HIAM-4009	Powder
		1.0 mL FA			-	-
23.3	10	0.5 mL AA	1.5 mL DMF	120 °C, 3 days	HIAM-4008	Powder
		1.0 mL AA			HIAM-4008	~10 μm
		1.5 mL AA			HIAM-4008	~60 μm
23.3	10	0.5 mL PA	1.5 mL DMF	120 °C, 3 days	HIAM-4008	Powder
		1.0 mL PA			HIAM-4008	~8 μm
		1.5 mL PA			HIAM-4008	~20 μm
23.3	10	200 mg BA	3.0 mL DMF	120 °C, 3 days	HIAM-4008	Powder
		500 mg BA			HIAM-4007	~20 μm
		700 mg BA			HIAM-4007	~50 μm
23.3	10	200 mg FBA	3.0 mL DMF	120 °C, 3 days	HIAM-4008	Powder
		500 mg FBA			HIAM-4007	~50 μm
		700 mg FBA			HIAM-4007	~70 μm

23.3	10	0.1 mL TFA	3.0 mL DMF	120 °C, 3 days	HIAM-4009	Powder
		0.2 mL TFA			HIAM-4009	~10 μm
		0.5 mL TFA			-	-
23.3	10	0.2 mL FA	2.0 mL DMA	120 °C, 3 days	HIAM-4008	~2 μm
		0.5 mL FA			HIAM-4009	~2 μm
		1.0 mL FA			-	-
23.3	10	0.5 mL AA	1.5 mL DMA	120 °C, 3 days	HIAM-4008	~2 μm
		1.0 mL AA			HIAM-4008	~15 μm
		1.5 mL AA			HIAM-4008	~10 μm
23.3	10	0.5 mL PA	1.5 mL DMA	120 °C, 3 days	HIAM-4008	~10 μm
		1.0 mL PA			HIAM-4008	~5 μm
		1.5 mL PA			HIAM-4008	~8 μm
23.3	10	200 mg BA	3.0 mL DMA	120 °C, 3 days	HIAM-4008	Powder
		500 mg BA			HIAM-4008	~30 μm
		700 mg BA			HIAM-4008	~40 μm
23.3	10	200 mg FBA	3.0 mL DMA	120 °C, 3 days	HIAM-4008	~2 μm
		500 mg FBA			HIAM-4008	~2 μm
		700 mg FBA			HIAM-4008	~15 μm
23.3	10	0.1 mL TFA	3.0 mL	120 °C, 3 days	-	-
		0.2 mL TFA	DMA		-	-

		0.5 mL TFA			-	-
23.3	10	0.2 mL FA	2.0 mL DEF	120 °C, 3 days	HIAM-4009	Powder
		0.5 mL FA			HIAM-4009	Powder
		1.0 mL FA			-	-
23.3	10	0.5 mL AA	1.5 mL DEF	120 °C, 3 days	HIAM-4008	~15 µm
		1.0 mL AA			HIAM-4008	~50 µm
		1.5 mL AA			HIAM-4008	~50 µm
23.3	10	0.5 mL PA	1.5 mL DEF	120 °C, 3 days	HIAM-4008	~15 µm
		1.0 mL PA			HIAM-4008	~20 µm
		1.5 mL PA			HIAM-4008	~25 µm
23.3	10	200 mg BA	3.0 mL DEF	120 °C, 3 days	HIAM-4009	~5 µm
		500 mg BA			HIAM-4009	~70 µm
		700 mg BA			HIAM-4009	~70 µm
23.3	10	200 mg FBA	3.0 mL DEF	120 °C, 3 days	HIAM-4009	~10 µm
		500 mg FBA			HIAM-4009	~20 µm
		700 mg FBA			HIAM-4009	~40 µm
23.3	10	0.1 mL TFA	3.0 mL DEF	120 °C, 3 days	HIAM-4009	~3 µm
		0.2 mL TFA			-	-
		0.5 mL TFA			-	-

Single crystal X-ray diffraction analyses

Single crystals of HIAM-4007 and HIAM-4008 were mounted on MicroMesh (MiTeGen) with paraton oil. The data were collected on a 'Bruker D8 VENTURE' diffractometer equipped with copper micro-focus X-ray sources ($\lambda = 1.5406 \text{ \AA}$). The crystals kept at the 250 K (HIAM-4007), 199 K (HIAM-4008) during data collection. Using Olex2², the structures were solved with the ShelXT³ structure solution program using Intrinsic Phasing and refined with the ShelXL⁴ refinement package using Least Squares minimization. In the structure HIAM-4007 and HIAM-4008, the amino groups of the APTC ligands are all disordered over two sites with site occupation factor of 0.5:0.5. Furtherly in HIAM-4008, six Zr^{4+} ions form an octahedron with the 8 faces each capped by a $\mu_3\text{-O}$ or $\mu_3\text{-OH}$. Eight of the edges of the octahedron are bridged by APTC ligands via bidentate carboxylate groups with the remaining four equatorial edges each bridged by a APTC ligand (occ = 0.5) that is monodentate to each equatorial Zr^{4+} center and bound through the carboxylate groups. The coordination sphere at the equatorial Zr^{4+} centers is completed by a terminal OH^- ligand. The amino groups of these monodentate disorder APTC ligand cannot be found from the residual electron density peaks. Disordered atoms were refined using geometry restrains (SADI, DFIX, FLAT), and restraints were also used to refine anisotropic displacement parameters of all non-hydrogen atoms (SIMU and DELU). The hydrogen atoms on the aromatic rings were located at geometrically calculated positions and refined by riding. However, the hydrogen atoms for the coordinated molecules cannot be found from the residual electron density peaks and the attempt of theoretical addition was not done. The free solvent molecules are highly disordered in HIAM-4007, and attempts to locate and refine the solvent peaks were unsuccessful. The diffused electron densities resulting from these

solvent molecules were removed using the SQUEEZE routine of PLATON⁵; structures were then refined again using the data generated. The B level alert for HIAM-4007 could be ascribed to its relative low diffraction intensity. The refinement results are summarized in Table S2-S3. Crystallographic data for all of the crystal structures in CIF format have been deposited in the Cambridge Crystallographic Data Centre (CCDC) under deposition numbers CCDC-2129023 (HIAM-4007), CCDC-2129024 (HIAM-4008). The data can be obtained free of charge via www.ccdc.cam.ac.uk/data_request/cif (or from the Cambridge Crystallographic Data Centre, 12 Union Road, Cambridge CB2 1EZ, U.K.)

N₂ sorption isotherms

N₂ sorption isotherms measurements were performed using a Micromeritics SFlex volumetric adsorption analyzer. As-synthesized HIAM-4007, HIAM-4008 and HIAM-4009 single crystals were washed with fresh DMF for one day to remove unreacted linkers and inorganic species. Then about 150 mg HIAM-4007, HIAM-4008 and HIAM-4009 were immersed into 16 mL DMF with 2 mL 8 M HCl, which was heated in an oven at 100°C for 16 hours. After cooling to room temperature, the supernatant solution was decanted and the resultant materials were washed using DMF for several times. Then fresh acetone was added and the samples were solvent-exchanged for 12 hours. This procedure was repeated for three times. Then the samples were dried under a dynamic vacuum under room temperature for 2 hours. Before adsorption measurement, the samples were further activated at 120°C for 12 hours. Low-pressure N₂ sorption isotherms were measured at 77 K in a liquid nitrogen bath. The surface areas were calculated using the Brunauer-Emmett-Teller model based on the N₂ sorption data.

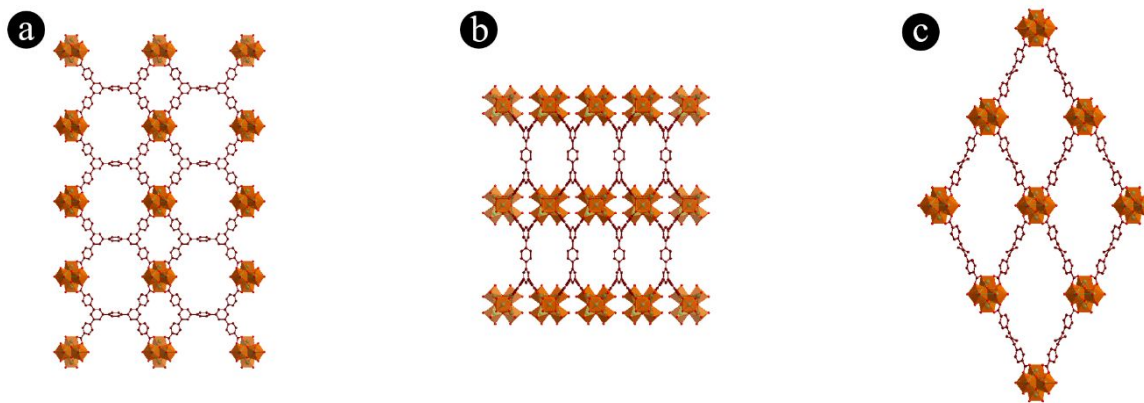


Figure S1. The single crystal structure of HIAM-4007 viewed along the *a* (a), *b* (b) and *c* (c) axis (color scheme: green, Zr; red, O; brown, C; brown, H and N atoms in the structures are omitted for clarity). For all node cluster description and underlying net (4,8)-c **scu**: <http://rcsr.net/nets/scu>.

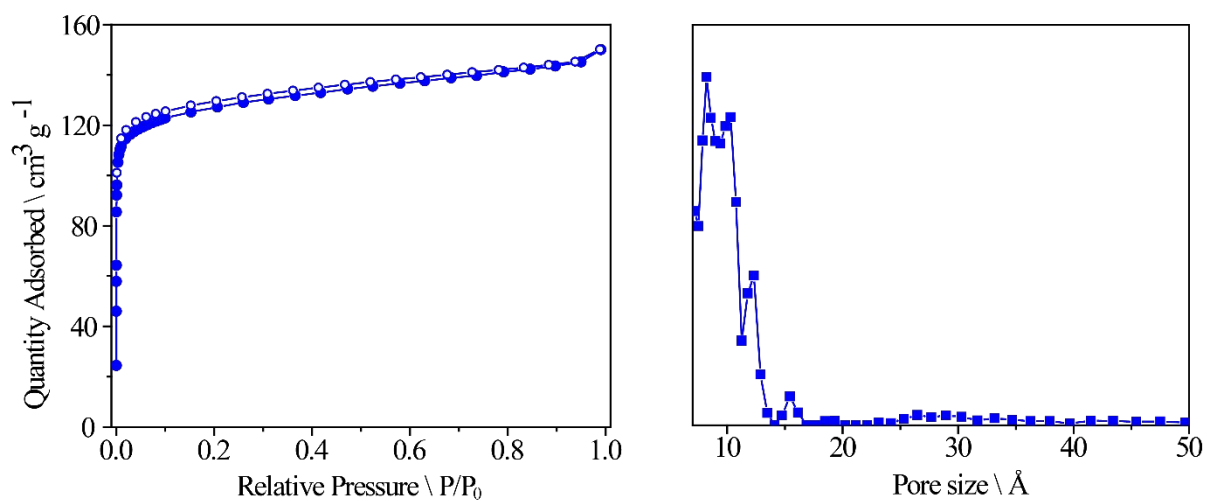


Figure S2. N_2 adsorption-desorption isotherms at 77 K (left) and pore size distribution (right) of HIAM-4007.

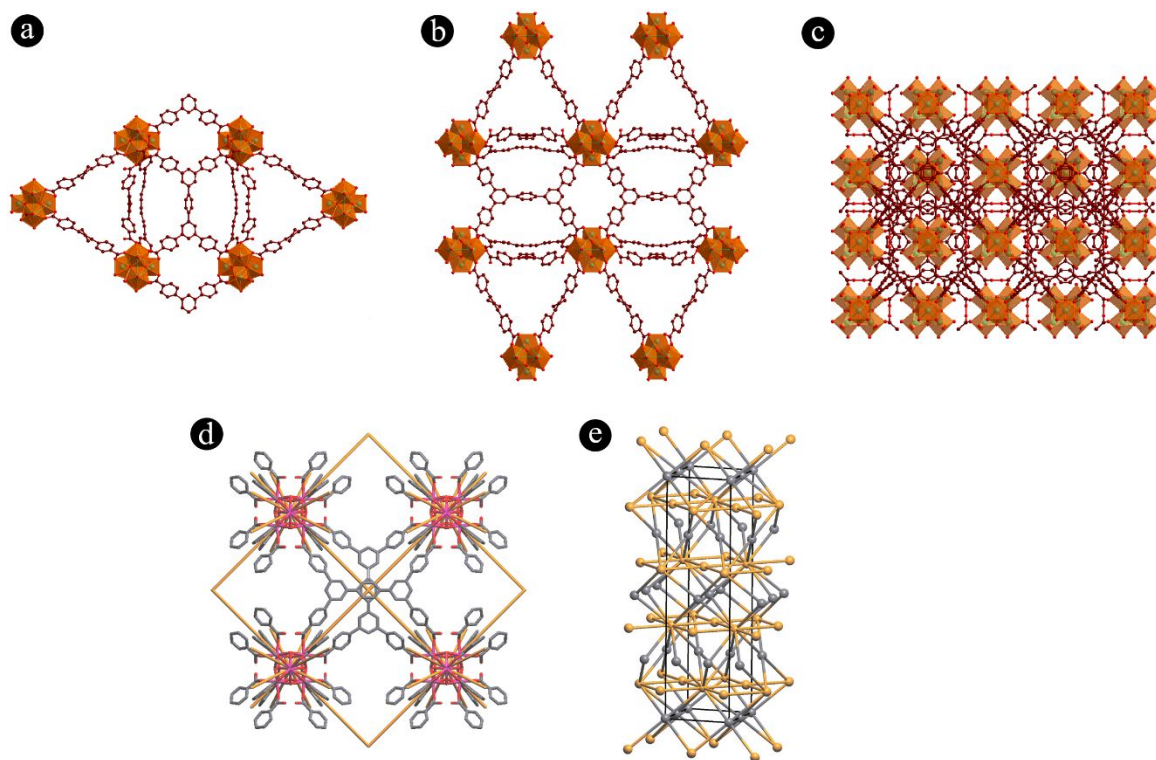


Figure S3. The single crystal structure of HIAM-4008 viewed along the *a* (a), *b* (b) and *c* (c) axis (color scheme: green, Zr; red, O; brown, C; brown, H and N atoms in the structures are omitted for clarity). For all node cluster description and underlying net (4,4,12)-c **scp**: <http://rcsr.net/nets/scp>. The 50%-50% disorder ligand behave as 4-coordinated node defining the orange **sql** layers of the **scp** net (d and e), raising the coordination of the Zr_6 cluster from 8 to 12-c.

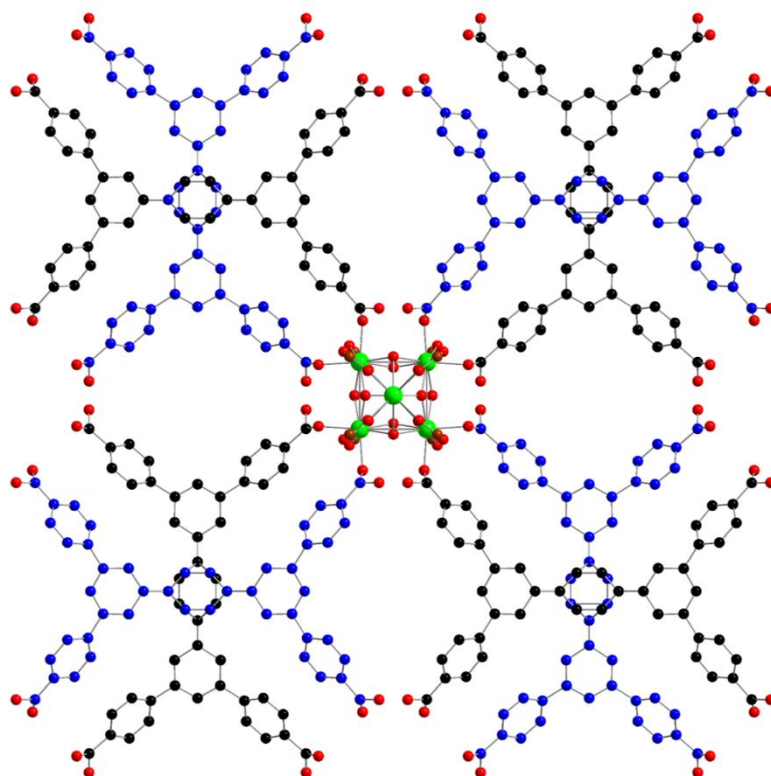


Figure S4. The eight disordered APTC in HIAM-4008 divided into two parts (the black part and the blue part) with occupancy of 50% for each part (hydrogen, amino groups and the ordered APTC were omitted for simplification).

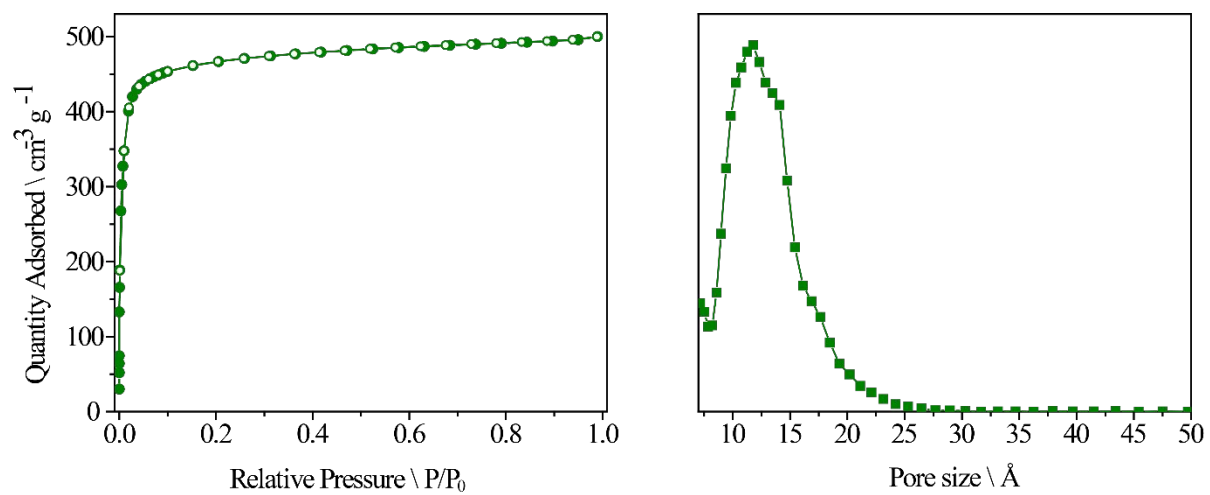


Figure S5. N₂ adsorption-desorption isotherms at 77 K (left) and pore size distribution (right) of HIAM-4008.

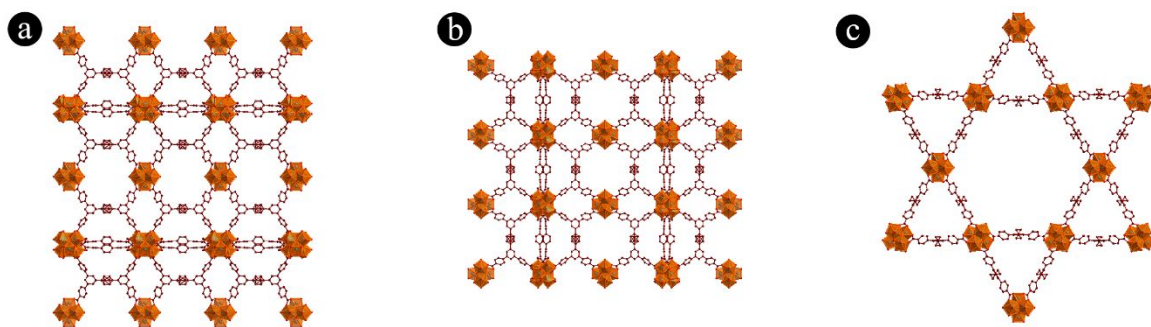


Figure S6. The structure of HIAM-4009 derived from PCN-808⁶ viewed along the *a* (a) and *b* (b) and *c* (c) axis (color scheme: green, Zr; red, O; brown, C; brown, H and N atoms in the structures are omitted for clarity). For all node cluster description and underlying net (4,8)-c **csq**: <http://rcsr.net/nets/csq>.

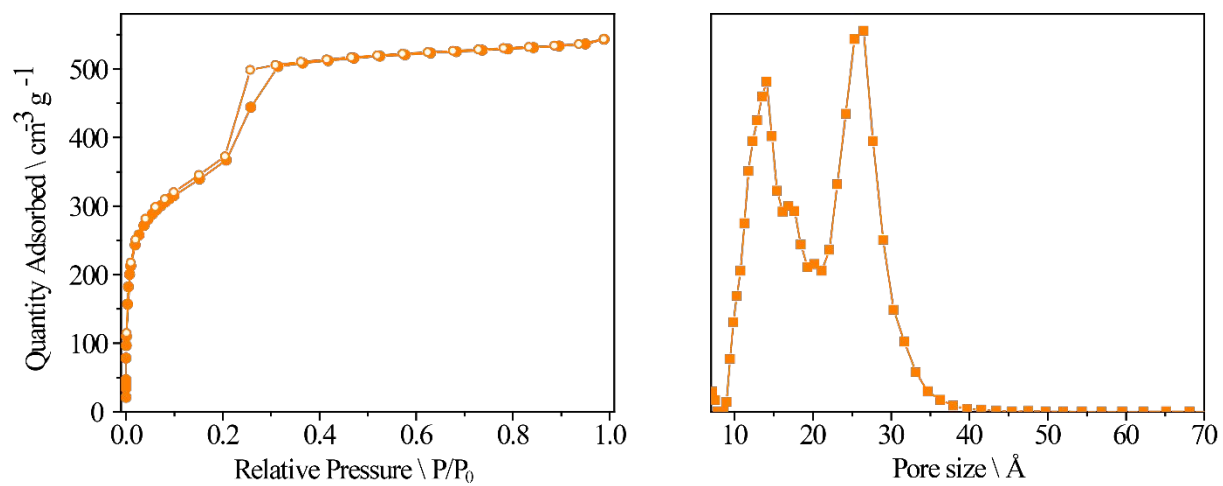


Figure S7. N₂ adsorption-desorption isotherms at 77 K (left) and pore size distribution (right) of HIAM-4009.

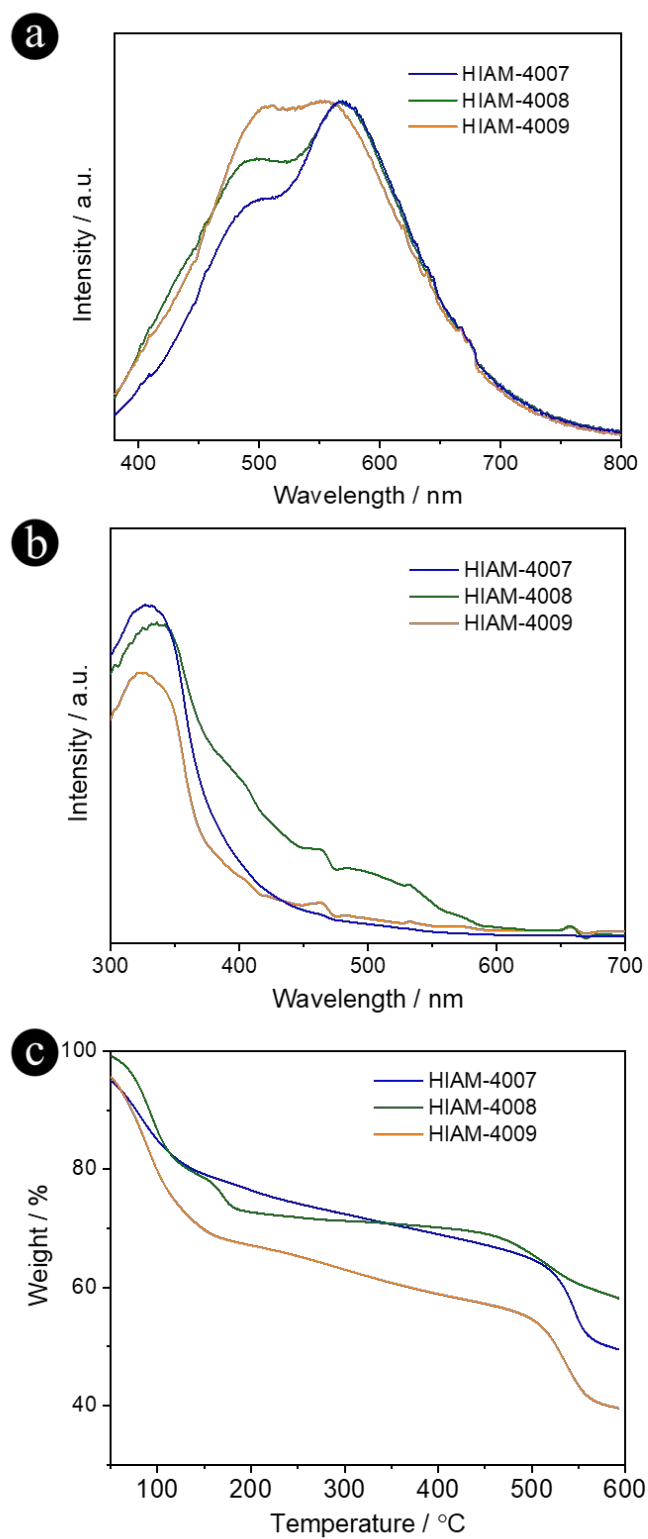


Figure S8. The normalized emission spectra (a), UV-vis absorption spectra (b) and (c) thermogravimetric (TG) profiles of HIAM-4007, HIAM-4008 and HIAM-4009.

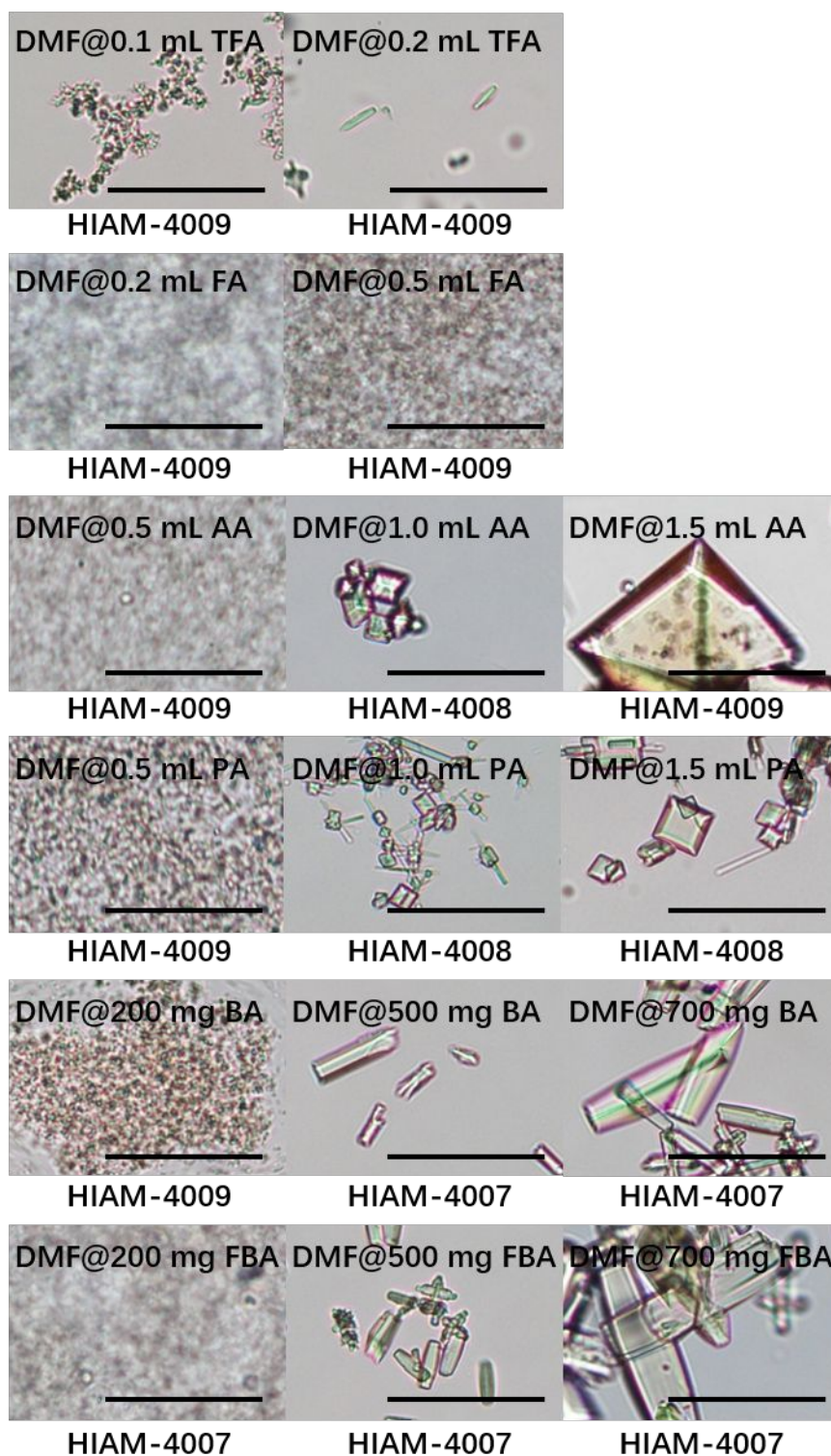


Figure S9. The single crystal images and types of MOFs obtained in the DMF with different acids under daylight (scale bar: 50 μ m).

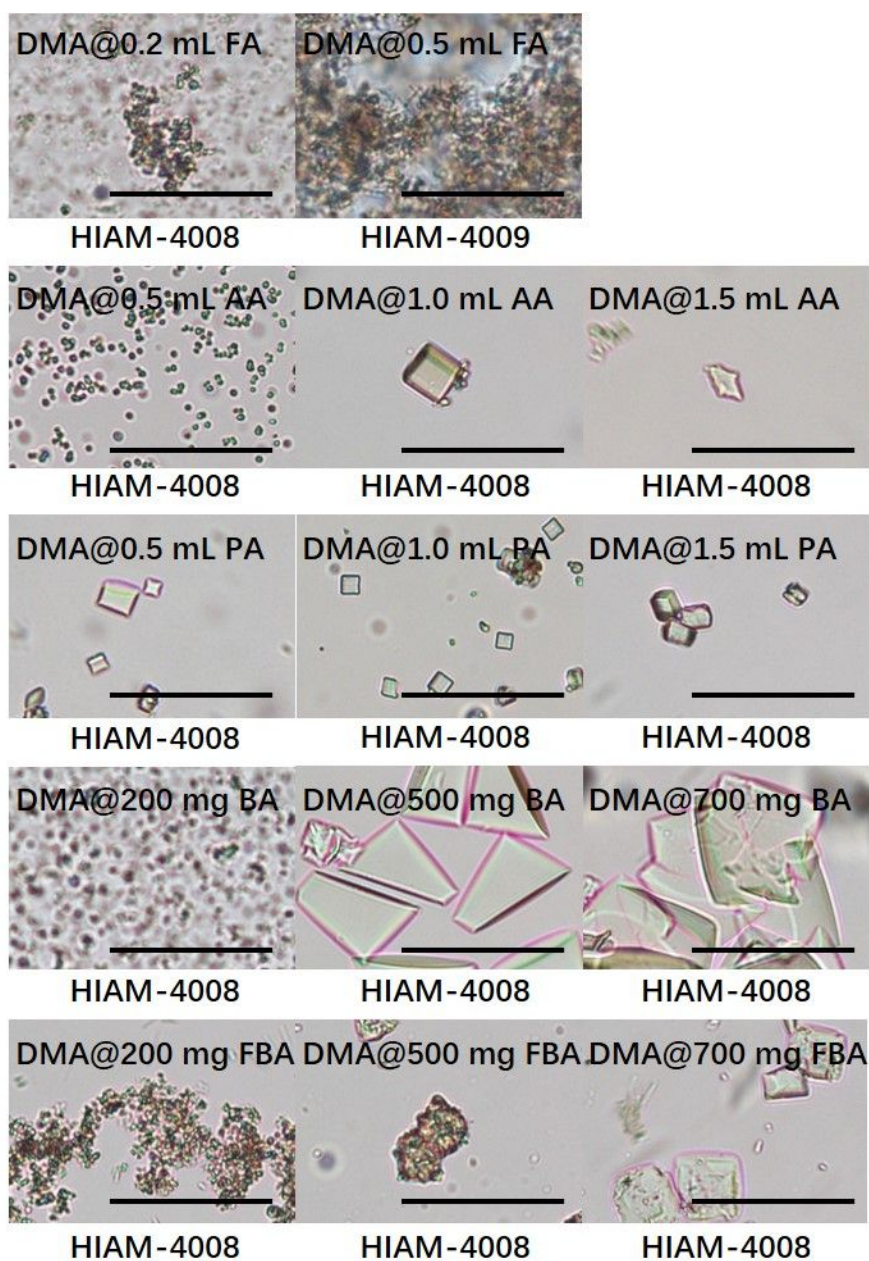


Figure S10. The single crystal images and types of MOFs obtained in the DMA with different acids under daylight (scale bar: 50 μ m).

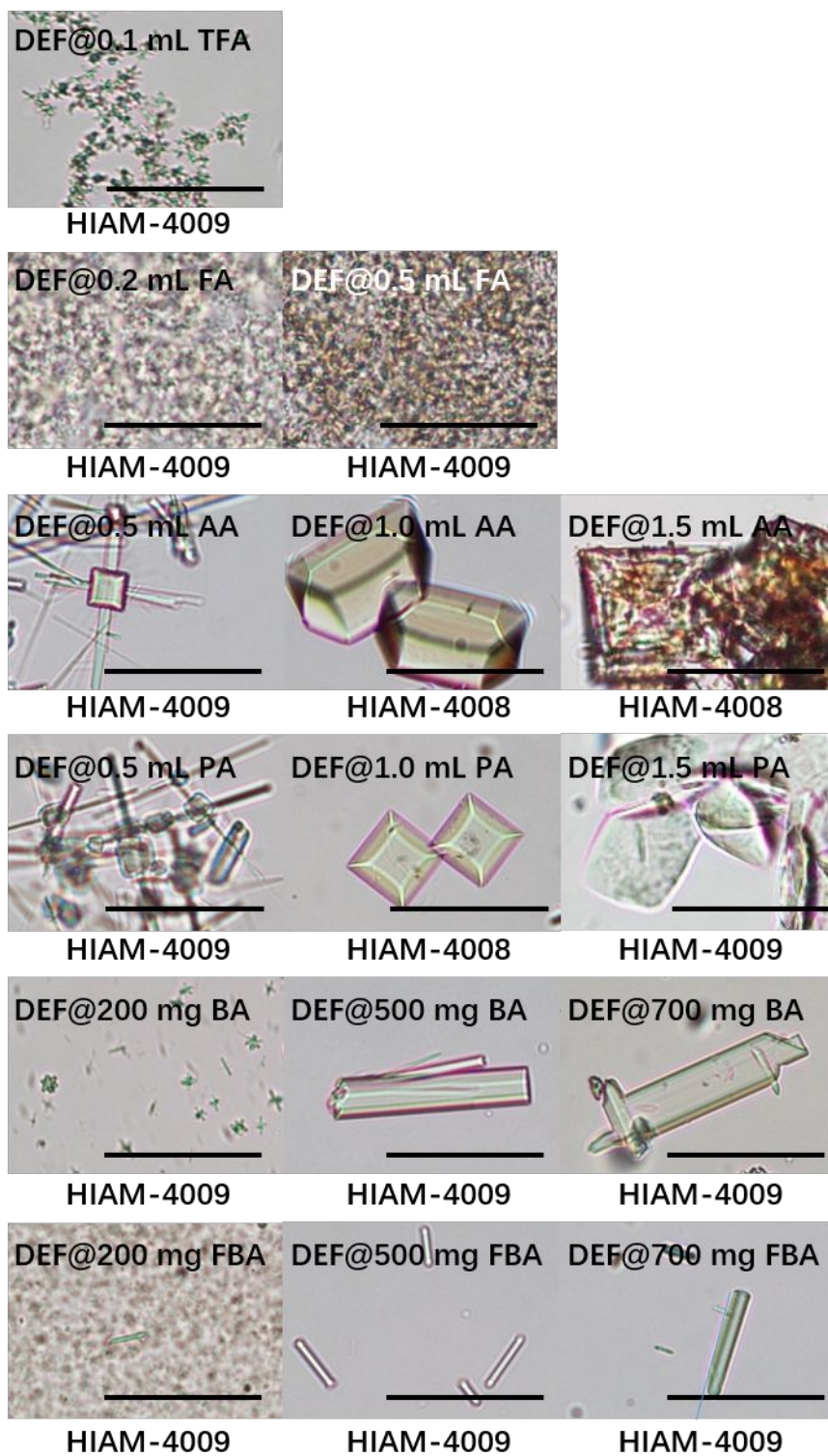


Figure S11. The single crystal images and types of MOFs obtained in the DEF with different acids under daylight (scale bar: 50 μm).

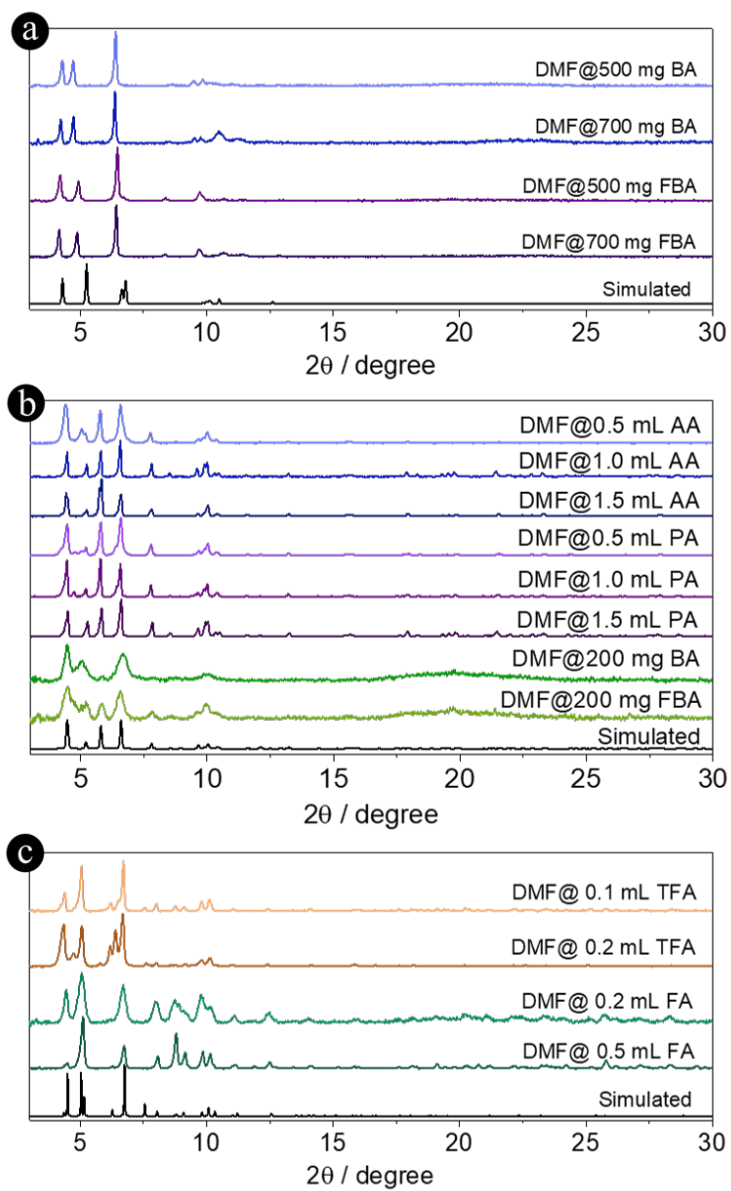


Figure S12. The PXRD patterns of HIAM-4007 (a), HIAM-4008(b) and HIAM-4009 (c) synthesized under different solvochemical conditions using DMF as solvent.

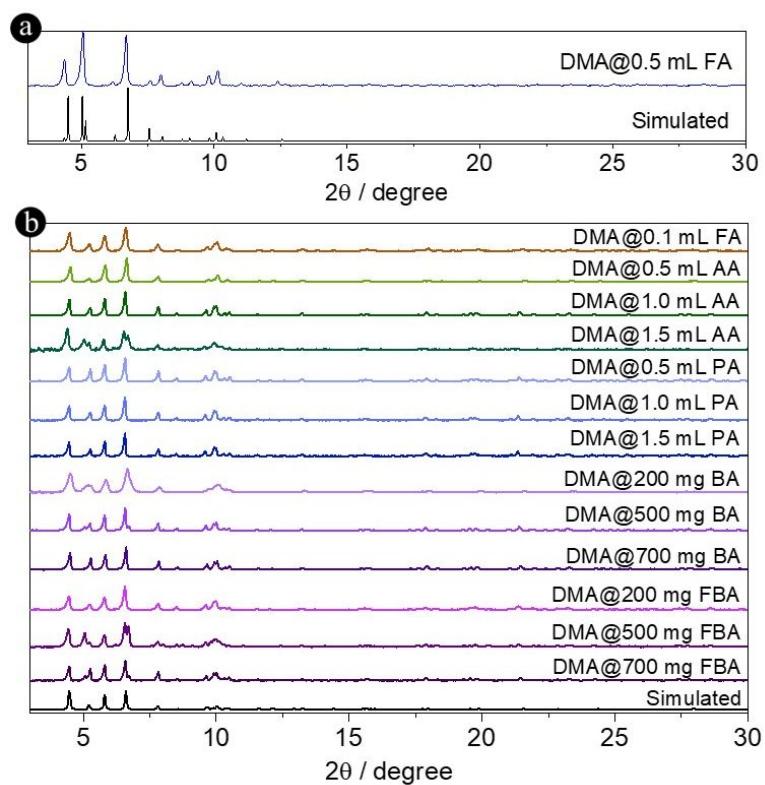


Figure S13. The PXRD patterns of HIAM-4009 (a) and HIAM-4008(b) synthesized under different solvothermal conditions using DMA as solvent.

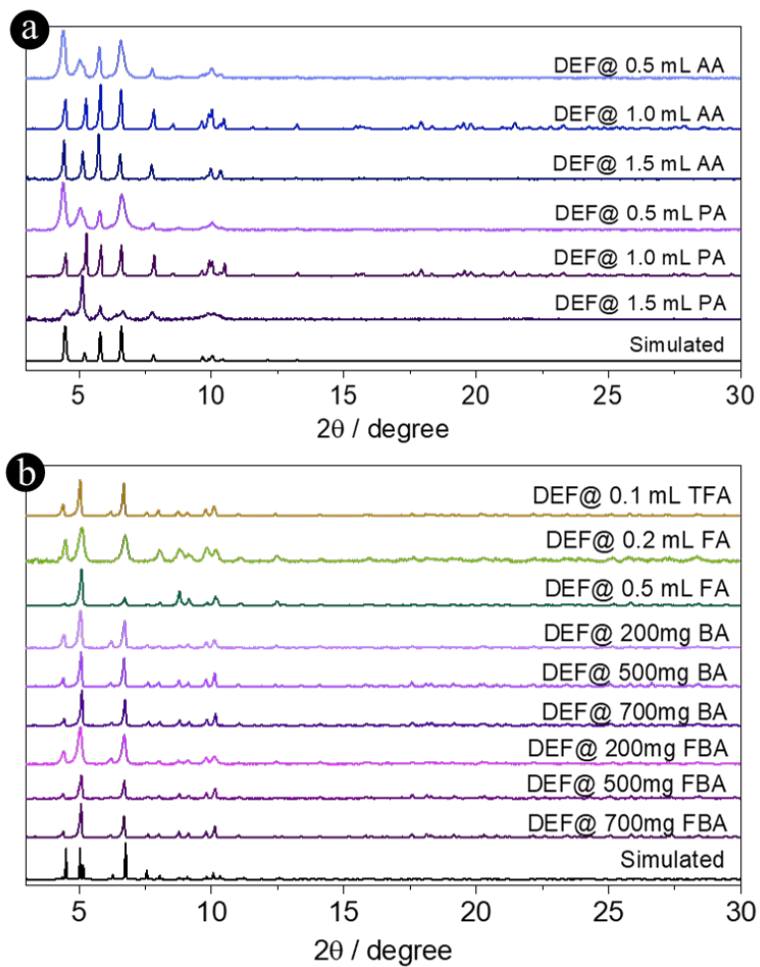


Figure S14. The PXRD patterns of HIAM-4008 (a) and HIAM-4009 (b) synthesized under different solvothermal conditions using DEF as solvent.

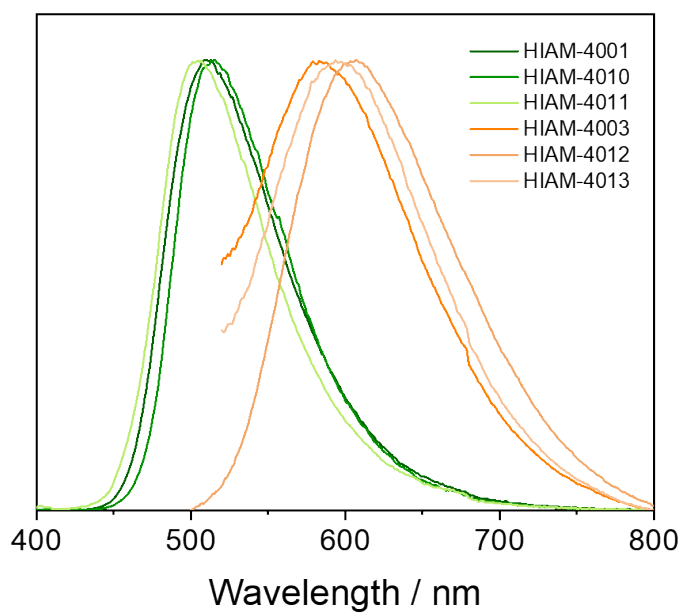


Figure S15. The normalized emission spectra of IAM-4001, IAM-4003, IAM-4010, IAM-4011, IAM-4012 and IAM-4013.

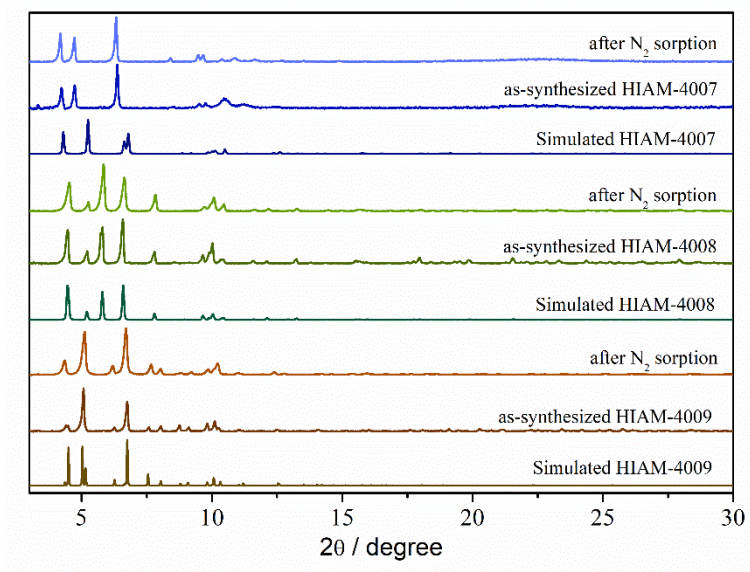


Figure S16. The PXR D patterns of simulated, as-synthesized and after N₂ sorption of HIAM-4007, HIAM-4008 and HIAM-4009.

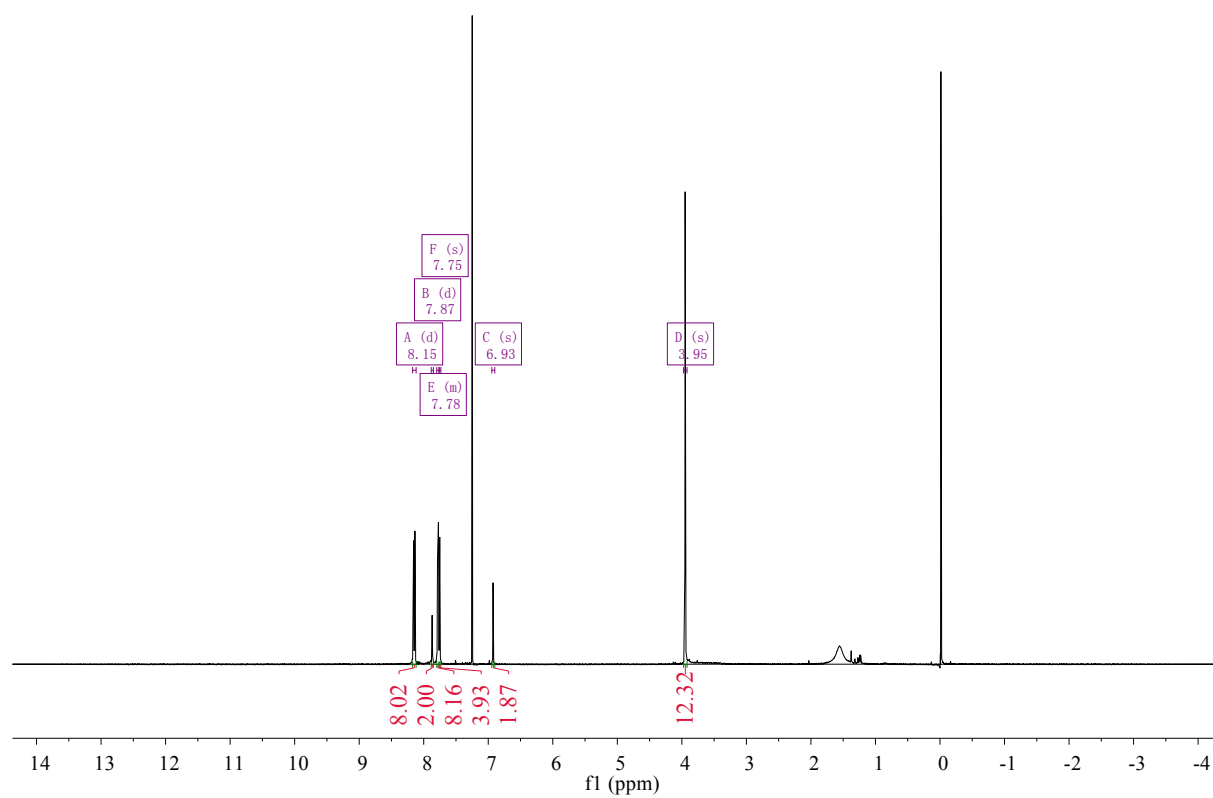


Figure S17. The ^1H NMR spectrum of tetramethyl 5',5'''-(2,3-diamino-1,4-phenylene)bis([1,1':3',1''-terphenyl]-4,4''-dicarboxylate) in CDCl_3 .

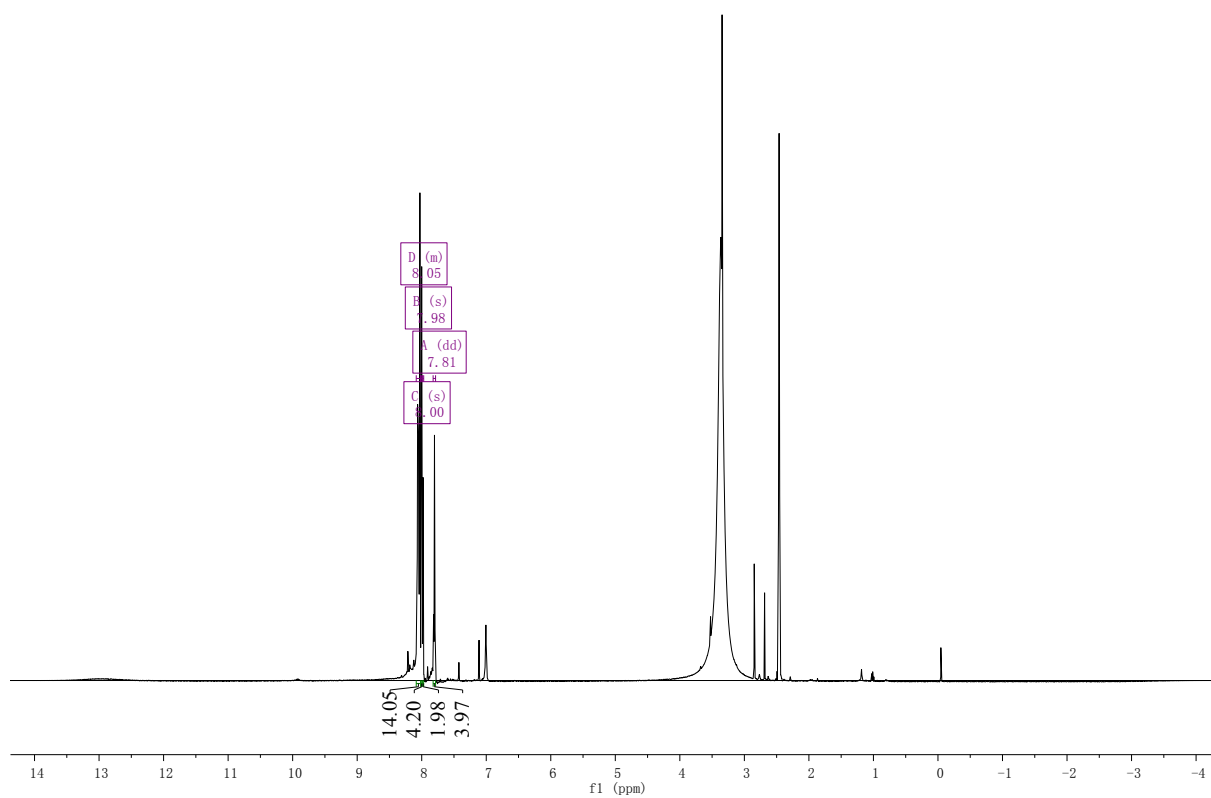


Figure S18. The ^1H NMR spectrum of APTC in $\text{DMSO-}d_6$.

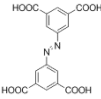

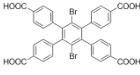


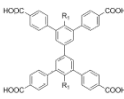


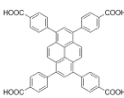


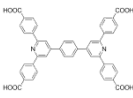


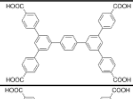

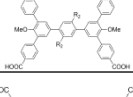

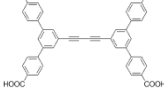

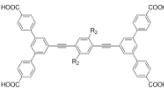

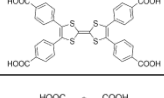

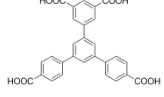

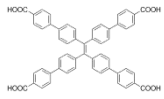

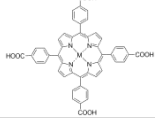


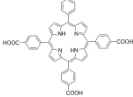

Table S2. Crystal data and structure refinement for HIAM-4007.

CCDC No.	2129023	
Empirical formula	C ₄₆ H ₂₂ N ₂ O ₁₆ Zr ₃	
Formula weight	1132.31	
Temperature	250 K	
Wavelength	1.54178 Å	
Crystal system	orthorhombic	
Space group	Cmmm	
Unit cell dimensions	a = 19.223(4) Å	$\alpha = 90^\circ$
	b = 35.032(5) Å	$\beta = 90^\circ$
	c = 20.525(3) Å	$\gamma = 90^\circ$
Volume	13821(4) Å ³	
Z	4	
Density (calculated)	0.544 g/cm ³	
Absorption coefficient	2.033 mm ⁻¹	
F(000)	2240.0	
Crystal size	0.100 x 0.050 x 0.050 mm ³	
Theta range for data collection	4.304 to 127.372°	
Index ranges	-22 ≤ h ≤ 12, -31 ≤ k ≤ 40, -20 ≤ l ≤ 23	
Reflections collected	22625	
Independent reflections	6117 [R(int) = 0.0985, R(sigma) = 0.0928]	
Data / restraints / parameters	6117 / 264 / 168	
Goodness-of-fit on F ²	0.950	
Final R indices [I > 2σ(I)]	R1 = 0.1100, wR2 = 0.2782	
R indices (all data)	R1 = 0.1523, wR2 = 0.3323	
Largest diff. peak and hole	1.33 and -0.92 e.Å ⁻³	

Table S3. Crystal data and structure refinement for HIAM-4008.

CCDC No.	2129024	
Empirical formula	C ₆₉ H ₃₅ N ₂ O ₁₈ Zr ₃	
Formula weight	1453.65	
Temperature	199 K	
Wavelength	1.54178 Å	
Crystal system	tetragonal	
Space group	I4 ₁ /amd	
Unit cell dimensions	a = 20.6505(4) Å	α = 90°
	b = 20.6505(4) Å	β = 90°
	c = 67.8228(12) Å	γ = 90°
Volume	28922.6(12) Å ³	
Z	8	
Density (calculated)	0.668 g/cm ³	
Absorption coefficient	2.018 mm ⁻¹	
F(000)	5816.0	
Crystal size	0.100 x 0.100 x 0.03 mm ³	
Theta range for data collection	7.798 to 136.7°	
Index ranges	-23 ≤ h ≤ 24, -24 ≤ k ≤ 22, -81 ≤ l ≤ 81	
Reflections collected	60210	
Independent reflections	7013 [R(int) = 0.0445, R(sigma) = 0.0204]	
Data / restraints / parameters	7013 / 141 / 289	
Goodness-of-fit on F ²	1.078	
Final R indices [I > 2σ(I)]	R1 = 0.0550, wR2 = 0.1787	
R indices (all data)	R1 = 0.0648, wR2 = 0.1917	
Largest diff. peak and hole	0.65 and -0.55 e.Å ⁻³	

Table S4. Tetratopic carboxylic acid-based Zr-MOFs with scu, sqc or csq topology.

Linker structure	Solvent	Acid	Topology (single node representation)	Status	MOF
	DMF	FA	scu		Zr-abtc ⁷
	DMF	AA	scu		NU-906 ⁸
	DEF	FA	csq		NU-1008 ⁸
	DMF	BA	scu		PCN-606 ⁹
	DMF	TFA	csq		PCN-608 ⁹
	DMF	BA	csq		NU-1000 ¹⁰
	DEF	BA	csq		NU-1000 ¹⁰
	DMF	BA	scp		MFM-600 ¹¹
	DMF	AA	sqc		BUT-15 ¹²
	DMF	AA	sqc		BUT-14 ¹²
	DMF	BA	csq		PCN-808 ⁶
	DMF	BA	scu		NPF-300 ¹³
	DEF	BA	csq		SIU-75 ¹⁴ SIU-100 ¹⁴
	DMF	BA	scu		Zr-TTFTB ¹⁵
	DMF	FA	csq		BUT-17 ¹⁶
	DMF	TFA	csq		PCN-128W ¹⁷
	DEF	BA	sqc		PCN-225 ¹⁸
	DEF	BA	csq		PCN-222 ¹⁹
	DMF	FA	csq		MOF-545 ²⁰

(reaction temperature: 120 °C; R₁ = OH, NH₂, OCH₃; R₂ = H, CF₃; 😊 indicates the solvent, acid and topology is consistent with the results observed in the present work; 😞 indicates different topology was obtained using the same solvent and acid).

References

1. Ren, D.; Xia, H.-L.; Zhou, K.; Wu, S.; Liu, X.-Y.; Wang, X.; Li, J., Tuning and Directing Energy Transfer in the Whole Visible Spectrum through Linker Installation in Metal–Organic Frameworks. *Angew. Chem. Int. Ed.* **2021**, *60* (47), 25048-25054.
2. Dolomanov, O.V., Bourhis, L.J., Gildea, R.J, Howard, J.A.K. & Puschmann, H. OLEX2: A Complete Structure Solution, Refinement and Analysis Program. *J. Appl. Cryst.* **2009**, *42*, 339.
3. Sheldrick, G.M. SHELXT-Integrated Space-Group and Crystal-Structure Determination. *Acta Cryst.* **2015**, A71, 3.
4. Sheldrick, G.M. Crystal Structure Refinement with SHELXL. *Acta Cryst.* **2015**, C71, 3-8.
5. Spek, A. L., Single-crystal structure validation with the program PLATON. *J. Appl. Cryst.* **2003**, *36*, 7-13.
6. Pang, J.; Di, Z.; Qin, J. S.; Yuan, S.; Lollar, C. T.; Li, J.; Zhang, P.; Wu, M.; Yuan, D.; Hong, M.; Zhou, H. C., Precisely Embedding Active Sites into a Mesoporous Zr-Framework through Linker Installation for High-Efficiency Photocatalysis. *J. Am. Chem. Soc.* **2020**, *142* (35), 15020–15026.
7. Wang, H.; Dong, X.; Lin, J.; Teat, S. J.; Jensen, S.; Cure, J.; Alexandrov, E. V.; Xia, Q.; Tan, K.; Wang, Q.; Olson, D. H.; Proserpio, D. M.; Chabal, Y. J.; Thonhauser, T.; Sun, J.; Han, Y.; Li, J., Topologically guided tuning of Zr-MOF pore structures for highly selective separation of C6 alkane isomers. *Nat. Commun.* **2018**, *9* (1), 1745.
8. Chen, Y.; Zhang, X.; Mian, M. R.; Son, F. A.; Zhang, K.; Cao, R.; Chen, Z.; Lee, S.-J.; Idrees, K. B.; Goetjen, T. A.; Lyu, J.; Li, P.; Xia, Q.; Li, Z.; Hupp, J. T.; Islamoglu, T.;

- Napolitano, A.; Peterson, G. W.; Farha, O. K., Structural Diversity of Zirconium Metal–Organic Frameworks and Effect on Adsorption of Toxic Chemicals. *J. Am. Chem. Soc.* **2020**, *142* (51), 21428-21438.
9. Pang, J.; Yuan, S.; Qin, J.; Liu, C.; Lollar, C.; Wu, M.; Yuan, D.; Zhou, H.-C.; Hong, M., Control the Structure of Zr-Tetracarboxylate Frameworks through Steric Tuning. *J. Am. Chem. Soc.* **2017**, *139* (46), 16939-16945.
10. Mondloch, J. E.; Bury, W.; Fairen-Jimenez, D.; Kwon, S.; DeMarco, E. J.; Weston, M. H.; Sarjeant, A. A.; Nguyen, S. T.; Stair, P. C.; Snurr, R. Q.; Farha, O. K.; Hupp, J. T., Vapor-Phase Metalation by Atomic Layer Deposition in a Metal–Organic Framework. *J. Am. Chem. Soc.* **2013**, *135* (28), 10294-10297.
11. Carter, J. H.; Han, X.; Moreau, F. Y.; da Silva, I.; Nevin, A.; Godfrey, H. G. W.; Tang, C. C.; Yang, S.; Schroder, M., Exceptional Adsorption and Binding of Sulfur Dioxide in a Robust Zirconium-Based Metal-Organic Framework. *J. Am. Chem. Soc.* **2018**, *140* (46), 15564-15567.
12. Wang, B.; Yang, Q.; Guo, C.; Sun, Y.; Xie, L. H.; Li, J. R., Stable Zr(IV)-Based Metal-Organic Frameworks with Predesigned Functionalized Ligands for Highly Selective Detection of Fe(III) Ions in Water. *ACS. Appl. Mater. Interfaces* **2017**, *9* (11), 10286-10295.
13. Zhang, X.; Frey, B. L.; Chen, Y. S.; Zhang, J., Topology-Guided Stepwise Insertion of Three Secondary Linkers in Zirconium Metal-Organic Frameworks. *J. Am. Chem. Soc.* **2018**, *140* (24), 7710-7715.
14. Yu, J.; Anderson, R.; Li, X.; Xu, W.; Goswami, S.; Rajasree, S. S.; Maindan, K.; Gomez-Gualdrón, D. A.; Deria, P., Improving Energy Transfer within Metal-Organic Frameworks by

Aligning Linker Transition Dipoles along the Framework Axis. *J. Am. Chem. Soc.* **2020**, *142* (25), 11192-11202.

15. Su, J.; Yuan, S.; Wang, T.; Lollar, C. T.; Zuo, J.-L.; Zhang, J.; Zhou, H.-C., Zirconium metal–organic frameworks incorporating tetrathiafulvalene linkers: robust and redox-active matrices for in situ confinement of metal nanoparticles. *Chem. Sci.* **2020**, *11* (7), 1918-1925.

16. Wang, B.; Wang, P.; Xie, L.-H.; Lin, R.-B.; Lv, J.; Li, J.-R.; Chen, B., A stable zirconium based metal-organic framework for specific recognition of representative polychlorinated dibenzo-p-dioxin molecules. *Nat. Commun.* **2019**, *10* (1), 3861.

17. Zhang, Q.; Su, J.; Feng, D.; Wei, Z.; Zou, X.; Zhou, H.-C., Piezofluorochromic Metal–Organic Framework: A Microscissor Lift. *J. Am. Chem. Soc.* **2015**, *137* (32), 10064-10067.

18. Jiang, H.-L.; Feng, D.; Wang, K.; Gu, Z.-Y.; Wei, Z.; Chen, Y.-P.; Zhou, H.-C., An Exceptionally Stable, Porphyrinic Zr Metal–Organic Framework Exhibiting pH-Dependent Fluorescence. *J. Am. Chem. Soc.* **2013**, *135* (37), 13934-13938.

19. Feng, D.; Gu, Z.-Y.; Li, J.-R.; Jiang, H.-L.; Wei, Z.; Zhou, H.-C., Zirconium-Metalloporphyrin PCN-222: Mesoporous Metal–Organic Frameworks with Ultrahigh Stability as Biomimetic Catalysts. *Angew. Chem. Int. Ed.* **2012**, *51* (41), 10307-10310.

20. Morris, W.; Voloskiy, B.; Demir, S.; Gándara, F.; McGrier, P. L.; Furukawa, H.; Cascio, D.; Stoddart, J. F.; Yaghi, O. M., Synthesis, Structure, and Metalation of Two New Highly Porous Zirconium Metal–Organic Frameworks. *Inorg. Chem.* **2012**, *51* (12), 6443-6445.